Range Enhancement of High Wing Piston Engine Aircraft by Drag Reduction Methodology

TABLE OF CONTENTS

Page

LIST OF GRAPHS

LIST OF FIGURES

Figure **Page**

ABSTRACT

Reduction in skin friction drag has always been a major concern to aerodynamicists, especially when streamlined body is flying at low angle of attack. This research evaluates the enhancement of skin friction drag due to rivets at cruise angle of attack for high-wing piston engine aircraft. Computational Fluid Dynamic analysis of wing with and without rivets was carried out to observe the difference occurring in total drag. Aircraft wing with chord of 1.35m and span of 0.31m with total of 334 round headed rivets of size 1/8" and 3/32" were modeled in CATIAv5. The protrusion of rivet after installation on the skin of wing was 1mm. Inverse D shaped domain constituting tetrahedral elements was modeled with 15c dimension for inlet and 20c dimension was selected behind trailing edge to capture true wake characteristics. In order to capture boundary layer effects unstructured mesh with grid refinement was carried out using inflation layer which kept y^+ of 30. ICEM CFD 16.0® was used for grid generation and numerical analysis was performed using commercially available software Fluent 16.0®. Velocity inlet, zero shear walls and pressure outlet were given as boundary conditions, whereas wing was modeled as wall with no slip condition. Steady viscous analysis was carried out at wide range angles of attack using SST k-ω model. Pressure-velocity coupling was ensured using SIMPLE (Semi-Implicit Method for Pressure Linked Equations) scheme and convergence criterion of $1x10^{-5}$ was set for residuals. CFD results were validated against $1/10^{th}$ model of aircraft using CAE subsonic wind tunnel facility. Inverse approach of component build up method for drag prediction was employed to calculate drag of wing section analytically. Results from CFD, wind tunnel and analytical solution were compared and found in reasonable agreement. Comparison of wing with and without rivets revealed that zero lift drag coefficient increased from 0.0220 to 0.0226 thereby decreasing L/D ratio from 2.136 to 2.205. Further by countersunk all rivets on wing, total drag could be decreased by 2.727% which could save 0.042 gallons of 100LL gasoline per sortie. Hence an increment of 4.2% in range and endurance could be envisaged in a sortie with gross takeoff weight of 1250Kg.

1. INTRODUCTION

Drag is one of four aerodynamic forces acting on aircraft to resist its motion against the fluid through which it is moving. The reduction of skin friction drag of military and commercial aerial vehicles has always been a major concern to aerodynamicists. Minimizing drag would increase the range as well as save the burden on foreign exchequer. Aerodynamic shapes having less protruding surfaces, mismatched surfaces and proper finished surfaces have less drag then blunt body. Lot of work is being done on reduction of drag to increase range and conserve fuel. Method of reducing drag is either let the flow on surface be as much laminar as it could be by delaying the transition. This can be achieved either through smooth surface or removing any protruding surface that forms the basis of transition. Rivets are protruding surfaces on aircraft, rivet itself are basis of drag by disturbing the airflow in the boundary layer causing skin friction drag.

2. LITERATURE REVIEW

2.1. Drag

Movement of any body through fluid is associated with some kind of opposing force that restricts its free movement. If that restricting force is not present the body is going to move continuously without any opposition and there won't be any energy losses. Its according to newton's third law of motion. In case of ball rolling over ground, frictional force is there to oppose its motion and hence forth. In case of aerial vehicles associated opposing force is called drag [1].

Drag has many types; each of them arises due to different reason. Parasite drag produced due to motion of body through fluid and is further categorized into form or pressure drag and skin friction drag. Sum of skin friction drag and form drag is also termed as profile drag.

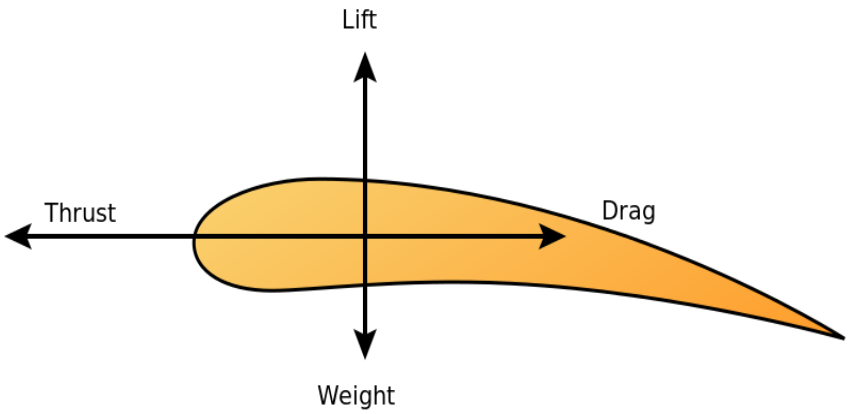

Figure 1 aerodynamic forces

Pressure drag arises due to shape of object. Blunt body will have more pressure drag as compared to aerodynamically smooth body. pressure drag directly relate with size of object. Object having larger cross section will having more drag as

compared to object of smaller cross section. The separation of air creates turbulence and results in pressure drag. Pressure drag is also known as form drag [2].

Skin friction drag arises when aircraft is flying in subsonic regime. it is the shear force which is caused by viscous airflow over the vehicle surface. It is a function of Reynold number, surface roughness. Making the body smooth will reduce the skin friction drag. Its origin is due to the contact of air particles with surface. More hinderance the particles will face in the motion, more will be skin friction drag [2].

Interference drag as name indicates it arises due to disturbance of flow when two surfaces meet with each other at perpendicular angle like wing and tail meets the fuselage. Turbulence arises due to surface which disrupts the flow.

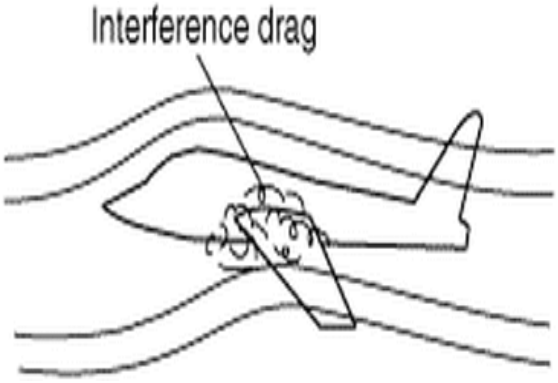

Figure 2 interference drag

Lift induced drag is produced as a creation of lift as flow passes over 3d body such as wing or fuselage of aircraft. This drag is mainly due to creation of vortices. Induced drag is directly proportional to the lift generated in a body. As wing's angle of attack increases, the lift coefficient increases as well so the drag due to lift increases until stall point is reached.

Wave drag is produced when body moves at speed of sound through a fluid. Wave drag is associated with shockwaves depending upon the speed of object. Shockwaves can be normal or oblique. It can also be called as compressibility drag.

2.2. Rivets

Assembly of aircraft require rivets. Rivets are permanent fasteners used to tie two components together. A rivet is a mechanical joint having cylindrical shape and a head. It's a permanent joint so it cannot be disassembled without failure of components. To insert a rivet a hole is created between two components where it is going to be applied and it exerts a force to hold two components together [3].

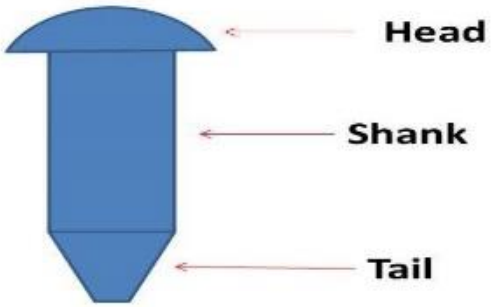

Figure 3 rivet

There is increase in drag due to protruding and countersunk rivet heads and surface roughness. The increase in drag caused by protruding rivets heads is roughly proportional to height of the heads. The method of reducing skin friction is the elimination of rivets heads, sheet-metal laps, other protruded surfaces and roughness from the surface exposed to air flow. Rivet head, being exposed to the airflow disturbs the flow in boundary layer and thereby increase the pressure drag

Type used

Rivets is an effective and cheaper way of joining two components. Depending on requirement, various shapes and sizes are available but in my case round headed rivet is used as shown

ROUND HEAD RIVET

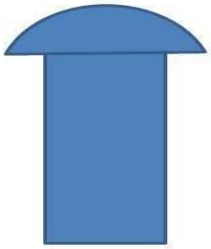

Figure 4 round head rivet

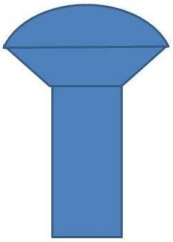

Figure 5 oval countersunk rivet head

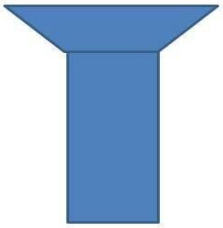

Figure 6 countersunk head rivet

2.3. NACA Rivet Report

Tests had been performed on aerofoil having 5ft chord. 8ft high speed tunnel was used for this purpose. The purpose of these tests was to determine the effect of exposed rivet heads on wing. The speed was varied from 80 to 500 miles per hour. Lift coefficient was varied from 0 to 0.30. Different types of rivets were used for this purpose to study the effect.

CONCLUSION

The increase in drag for 5 ft aerofoil varied from 6 percent due to counter sunk rivets, 27 percent due to 3/32-inch brazier-head rivets. The result was, drag increased by protruding rivet is roughly proportional to height of rivet head. Changes in span wise arrangement of rivets keeping the number of rivets same would result is variation of drag. Removing the rivets from the forward 30 percent of chord of aero foil reduce the rivet drag by 70 percent.

2.4. Paint Coating

Paint not only amplifies the aesthetics of aircraft but a good coating of paint is applied with the intent of reducing skin friction drag. Skin friction drag will increase as a result of surface roughness due to surface imperfections or mismatches or adhesion of dirt or dead insects sticked to surface or any other contaminations present caused as a result of oil leaks, spillage or de-icing. Paint coatings may provide some degree of drag reduction. Many coatings are composed of Nano particles which are small enough to fill even the tiniest of cracks or imperfections present on surface. Good coating will reduce the chances of adhesion of dust particles resulting in less skin friction drag.

2.5. Boeing Report

Boeing has done extensive research on how to decrease the fuel cost by decreasing the drag. They found out that having good coating of paint not only delays the transition point, laminar to turbulent flow transition but also reduces the skin friction drag by increasing the smoothness of surface. Surface coating would

promote the laminar flow. Laminar flow is characterized by more orderly flow of air particles thus having less skin friction drag then turbulent flow which is accompanied by irregular flow eddies. Surface irregularities can cause the boundary layer to transit from laminar to turbulent. If the finished skins on airplanes of aluminum and composites are hydraulically smooth then very little additional roughness drag can be accessed beyond normal skin. Surface coatings even reduce washing requirement for aircrafts because smooth surface wont aid in adhesion of dust particles and result in reduced excrescence drag [6].

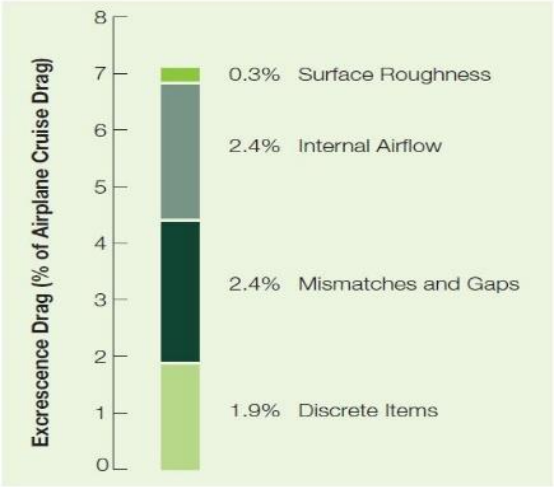

Figure 7 drag quantification from Boeing report

2.6. Methods of reducing drags

SUCTION METHOD

One method as already discussed of reducing skin friction drag is to delay the transition on wetted surface as much as possible. This approach is followed in controlling laminar controlling programs and other method is using suction walls. It may be in form of distributed porosity over surface or in form of series of span wise running slots. It is not effective to fully control the turbulence but effective enough to maintain laminar flow to some extent by maintaining the laminar velocity profile. It may stop the amplification that may leads to instability that leads to growth of

turbulence. This way local friction can be reduced to up to 20 percent of its turbulent value.

Location of first suction pore greatly depend upon the fact that one knows where transition going to be occur. At low altitudes dirt adhesion of insect cause the turbulence.

NATURAL LAMINAR FLOW

Another technique for maintaining the laminar flow over wing is to create favorable pressure gradients. This can be achieved without any suction wall or disturbing the structural integrity but just by bringing the point of maximum thickness as far as possible to create gradients of favorable pressure.

HYBRID LAMINAR FLOW

This can be done by using the two methods mentioned above by combining the maximum thickness as well as suction pores to achieve laminar flow to much as extent as possible.

WALL COOLING

Physical technique of wall cooling can be used to maintain laminar flow. Reduction in skin surface temperature would increases in the minimum critical Reynold number. Heat source would modify the viscosity distribution across the boundary layer which caused the turbulent flow. Liquid hydrogen can be used for this purpose. The fuel would be circulated below the wing surface cooling the surface and changing viscosity distribution.

ACTIVE WAVE SUPPRESSION

A passive method is tested in laboratory. it works on the principle of super positioning by active cancellation or suppression of any low magnitude wave that causes instability. The idea is to generate a wave of equal in magnitude but opposite in direction that would cancel out the effect of incoming instability. The

generated wave would be in 180-degree phase shift. It can be implemented for low subsonic flights [9].

2.7. Methods of evaluating

WIND TUNNEL

In wind tunnel testing an environment is simulated in wind tunnel that is similar to actual flow conditions to study the aerodynamic parameters like lift or drag. On the basis of shape and speed of flow wind tunnels are classified into open and close wind tunnel. In CAE, close wind tunnel is present.

For wind tunnel testing there are four similarity parameters which need to be considered which include Mach number, Froude's number, Mach number and geometric similarity between actual aircraft and model [4].

Figure 8 CAE wind tunnel

COMPUTATIONAL FLUID DYNAMICS (CFD)

The other method is using CFD. In CFD a virtual environment is created by plugging in all the environmental conditions and boundary conditions, then aerodynamic parameter is studied. The accuracy of results obtained depend upon the conditions and parameters imposed and computational power available. CFD is cheaper as well as faster approach.

Working of CFD

Discretization method is used in CFD for solving the equations governing the fluid mechanics. At each node these algebraic equations are solve simultaneously to provide the solution. For this purpose, a grid has to be refined to get accurate results. The accuracy of results depends upon the grid generated. More refined grid means more computational power would be needed [5].

2.8. Previous Work

Earlier CFD analysis has been done but that didn't include the effect of rivets or other protruding surfaces. To study the effect of these surfaces, an undergraduate project is launched. CFD analysis to find out the stability was also done including the propeller effect but it also didn't include rivets effect.

3. METHODOLOGY

The methodology has following steps

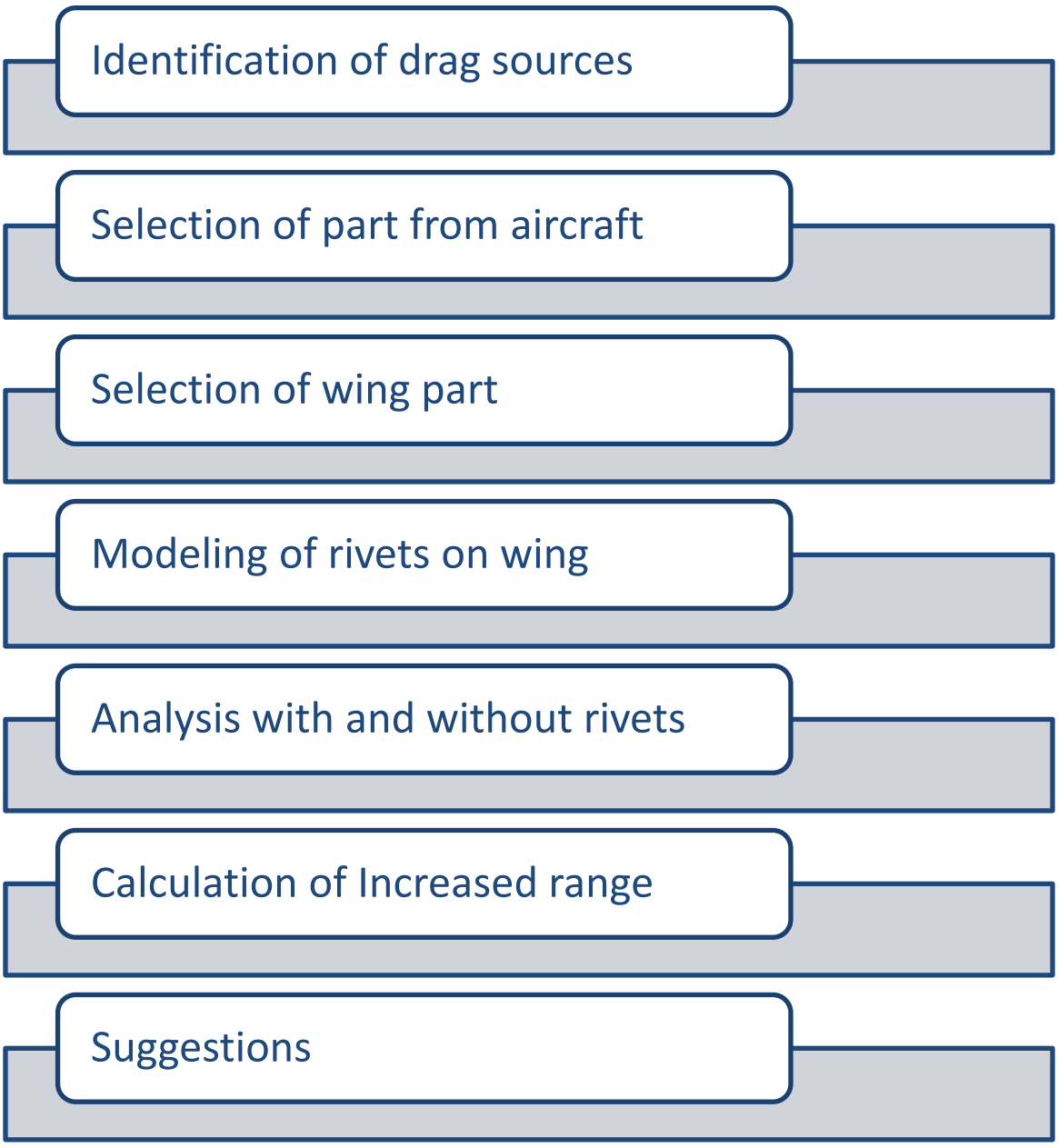

3.1. Observation of drag areas

Mismatches

Mismatched surfaces contribute towards disturbing the flow. Making the transition from laminar to turbulent.

Figure 9 mismatches of panels

Rough surface

rough surfaces due to adhesion of dirt or corrosion would result in drag. A good coating of paint removes this problem.

Figure 10 rough surfaces on body

Protruding surfaces

Protruding surfaces are major cause of disturbance of the smoothness of flow. Many protruding surfaces are present over the body.

Figure 11 protruding surfaces in body

Rivets

Round headed rivets of two sizes are used of 1/8 inch and 3/32 inch. Shown below are rivets on fuselage.

Figure 12 rivets

3.2. Selection of part

As CFD of whole aircraft with rivets cannot be done It would require a lot of computational power. In order to reduce the problem and find an effective solution for minimizing drag. I decided to select part of aircraft and quantify the effect of rivets on that part and see how much that part contribute in skin friction drag and pressure drag.

3.3. Modelling of Part

Span of wing is 8.84m. whole wing cannot be used for quantification due to computational power so span of 0.31m was selected with total number of 334 rivets. That part would quantify the effect of rivets on whole wing. Round head rivets are present on the surface of wing. There are two sizes of rivet one is 1/8 and other is 3/32 inch whose protrusion after installment on skin of in 1mm.

3.4. Quantification

Comparison between part with and without the rivets would indicate the difference in drag. That results would be compared and would be used for whole surface to find the exact amount of drag on that part.

3.5. Grid generation

Reynold number is calculated first to check either the flow is laminar or turbulent. In case of turbulent flow boundary layer effects need to be catered. For that purpose, Y^+ is used. Depending upon the computational power available and turbulent model selected Y^+ value is decided. Y^+ is a non-dimensional parameter used when calculating the height of first layer used in inflation layer. Inflation layer is used when boundary layer effects need to be observed.

3.6. Turbulent Models

Spalart-Allmaras model (SA)

This is one equation model. It is used when fast convergence and less accuracy is required. It is specifically suited for aerospace applications having boundary layer for study of adverse pressure gradient. It finds its application also in turbomachinery. It is effective when Reynold number is low.

$$\frac{\partial(\rho\epsilon)}{\partial t} + \frac{\partial(\rho\epsilon u_i)}{\partial x_i} = \frac{\partial}{\partial x_j}\left[\frac{\mu_t}{\sigma_\epsilon}\frac{\partial \epsilon}{\partial x_j}\right] + C_{1\epsilon}\frac{\epsilon}{k}2\mu_t E_{ij}E_{ij} - C_{2\epsilon}\rho\frac{\epsilon^2}{k}$$

K-EPSILON MODEL

k-epsilon mode is commonly used turbulent model, it's a two-equation model. It includes two extra transport equations to solve turbulent properties of flow. K is turbulent kinetic energy and epsilon is turbulent dissipation.

For turbulent kinetic energy

$$\frac{\partial}{\partial t}(\rho\tilde{\nu})+\frac{\partial}{\partial x_i}(\rho\tilde{\nu}u_i)=G_\nu+\frac{1}{\sigma_{\tilde{\nu}}}\left[\frac{\partial}{\partial x_j}\left\{(\mu+\rho\tilde{\nu})\frac{\partial\tilde{\nu}}{\partial x_j}\right\}+C_{b2}\rho\left(\frac{\partial\tilde{\nu}}{\partial x_j}\right)^2\right]-Y_\nu+S_{\tilde{\nu}}$$

For turbulent dissipation energy

$$\frac{\partial(\rho k)}{\partial t}+\frac{\partial(\rho k u_i)}{\partial x_i}=\frac{\partial}{\partial x_j}\left[\frac{\mu_t}{\sigma_k}\frac{\partial k}{\partial x_j}\right]+2\mu_t E_{ij}E_{ij}-\rho\epsilon$$

SST KW MODEL

SST k-w model is becoming popular because of extensive use in boundary layer as it combines two-equation eddy-viscosity model. it consists of standard k-w and transformed k-e model which are multiplied by blending function then both models are added together. The value of function is zero near wall region thus activating k-w I that zone. When away from surface the value of this function is zero thus activating k-e model. moreover, turbulent viscosity is modified to account for transport of turbulent shear stress. Its best suited for adverse pressure gradient and for aerofoil which have formation of boundary layer around. So, in order to resolve the effects of rivet in boundary layer shear stress transport k-w model was used. SST k-w resolves the boundary layer in greater detail as compared to SA model or k-epsilon model as it contains modified turbulent viscosity.

Turbulent kinetic energy

$$\frac{\partial k}{\partial t}+U_j\frac{\partial k}{\partial x_j}=P_k-\beta^*k\omega+\frac{\partial}{\partial x_j}\left[(\nu+\sigma_k\nu_T)\frac{\partial k}{\partial x_j}\right]$$

Specific dissipation rate

$$\frac{\partial\omega}{\partial t}+U_j\frac{\partial\omega}{\partial x_j}=\alpha S^2-\beta\omega^2+\frac{\partial}{\partial x_j}\left[(\nu+\sigma_\omega\nu_T)\frac{\partial\omega}{\partial x_j}\right]+2(1-F_1)\sigma_{\omega2}\frac{1}{\omega}\frac{\partial k}{\partial x_i}\frac{\partial\omega}{\partial x_i}$$

3.7. Boundary conditions

a. Velocity inlet

This boundary condition is used to define velocity direction and its scalar components of flow at inlet boundaries.

b. Pressure outlet

Pressure outlet is used to define pressure at inlet or outlet boundaries provided we know the values of pressure. We are defining the static pressure acting at boundaries

c. Pressure Far field

This boundary condition is used for boundaries that are located at distance that does not have impact on body which is under observation. Normally these boundaries are very far from object.

1) Initialization

Before staring a solution in fluent initial guess values are provided that would provide an estimated solution. Two types of initialization are there

a. Hybrid initialization

In hybrid initialization uses Laplace's equation to determine velocity and pressure. Variables such as temperature, pressure, turbulence are patched automatically based on domain averaged values or using interpolation [10].

b. Standard initialization

Unlike as in hybrid initialization values are provided in standard initialization. Zone name is selected from where the solution is to be initialized and values are provided for variables.

2) Monitors

Monitors include drag, lift and moment monitors. Its applied for study of these effects on surface under observation.

3.8. Range calculations

Using Breguet range equation the range of aircraft will be calculated

$$Range = \frac{V\ (L/D)}{g.SFC} ln \frac{W_{initial}}{W_{final}}$$

Before and after modification range would be compared to see the increased range. For range enhancement weight, velocity and gravitational pull remains constant. The only factor varying would be L/D. In order to maximize the range L/D has to be made greater which would be done by countersunk all the rivets. Hence decreasing the drag thereby increasing the L/D and increasing the range.

4. SETUP

In order to observe difference between drag in case of clean wing and riveted wing Computational Fluid Dynamics (CFD) was carried out along with analytic prove as well as experimental validation was carried out.

4.1. Selection of wing

Wing span of aircraft considered is 8.84m and mean aerodynamic chord is of 1.35m. whole wing span cannot be selected for analysis due to computational power available. As the total span consist of total of 9,524 round headed rivets which make it impossible to model in Catia with exact pattern. To solve this difficulty instead of whole wing; span of 0.31m was selected. The selection was based on the repetitive pattern of rivets on wing. After every 0.31m there was similar pattern constituting total of 334 rivets of 3/32 and 1/8-inch sizes. the protrusion of rivet after installment on wing skin came out to be 1mm. To capture the effect of rivets the element size has to be smaller than rivet size. If whole wing was modeled and afterwards the grid would be so dense that a lot of computational power would be required so span of 0.31m solves the problem.

4.2. CFD

Catia modeling

The name of aerofoil was unknown so the cad model provided was used to extract the aerofoil then extrude the wing. Using 3d projection in Catia the aerofoil was extracted. Then the job was to model rivets with exact spacing and sizes. there were two different rivets. Due to curved surface a pattern could not be generated so it was tedious job, finally, the wing with rivets was obtained.

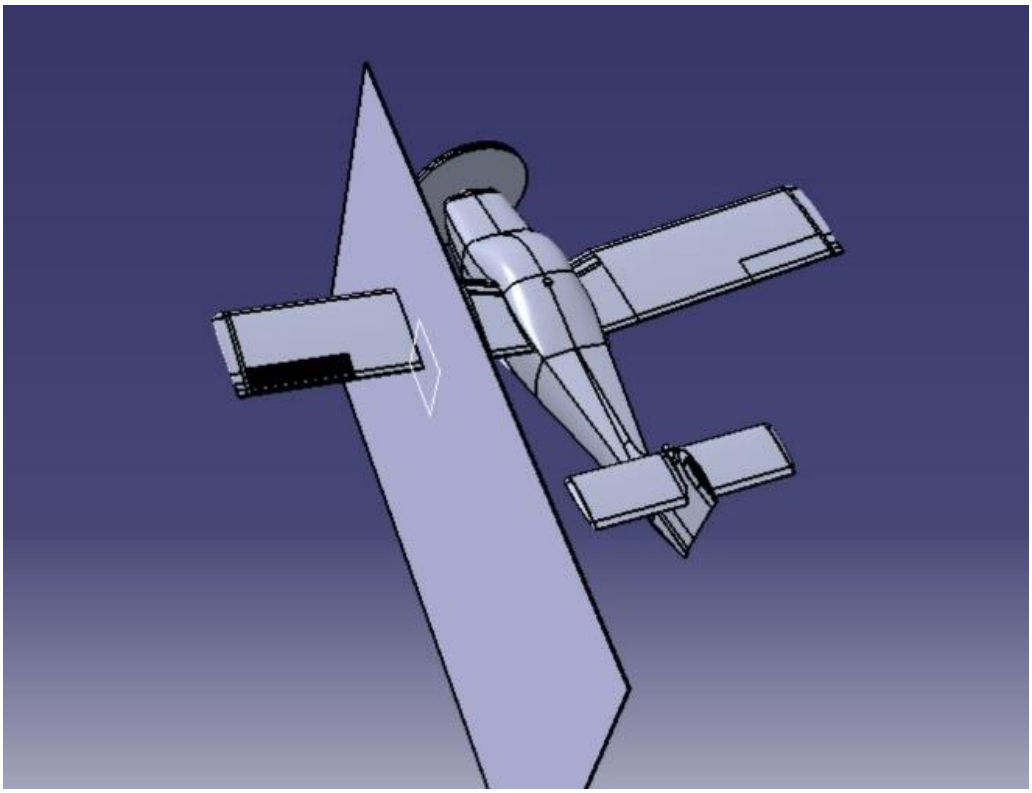

Figure 13 section plane

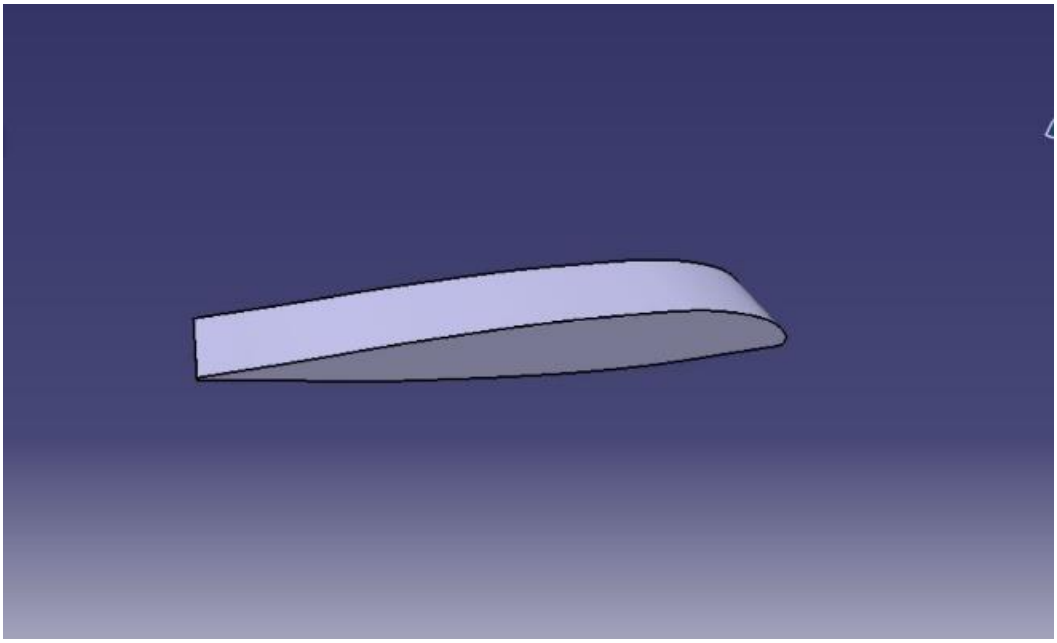

Figure 14 clean wing

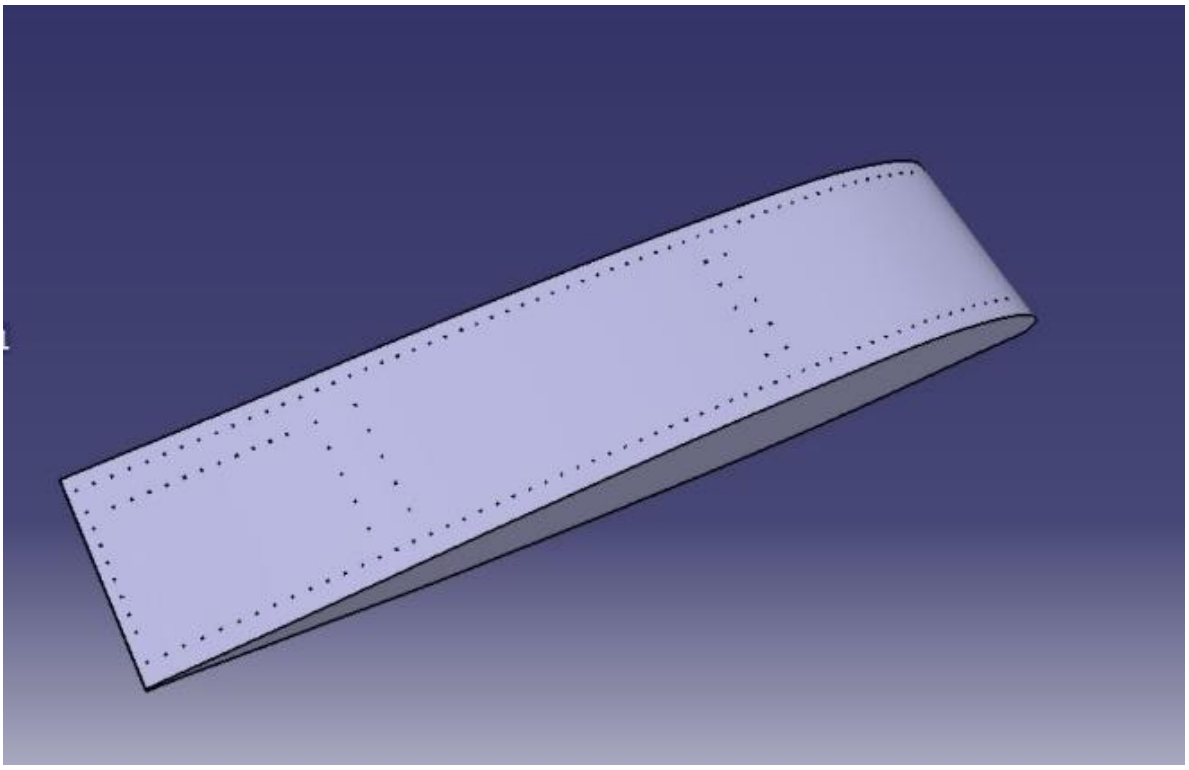

Figure 15 Riveted wing

Parameters

Analysis was carried out at sea level conditions using cruise velocity of 66.67m/s.

Density = 1.224691 kg/m^3

Pressure = 101325 N/m^2 (Pa)

Viscosity = 17.93 e-6 kg/m/s

Domain

Most important thing in CFD is domain selection. In this case and inverse D shaped domain having 15c dimension ahead of wing and 15c dimension from top and bottom wall so that the domain walls don't have any effect on wing. In order to capture the characteristics of wake 20c dimension was given after trailing edge.

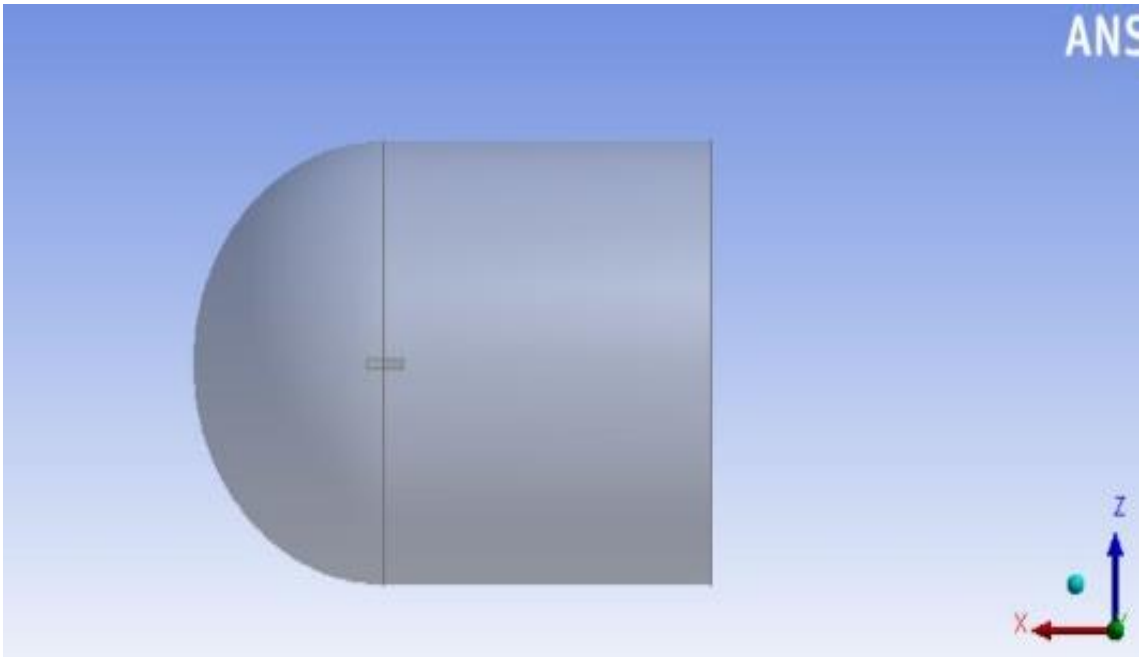

Figure 16 domain shape and size

in order to model the domain, the wing was imported from CATIA then using plane a sketch was drawn and it was revolved around x-axis to get bullet shape or inverse D-shaped domain.

4.2.1. Clean wing analysis

Grid generation

To compare the effects and differentiate the drag, analysis of clean wing was first done. As the geometry has already been created using Catia. Grid generation was done using ICEM CFD. As ICEM CFD works on binary algorithm, so leading edge and trailing edge was given size of 1/512 while the remaining surface was given size of 1/256. This way surface mesh was generated using all tri elements and patch independent method.

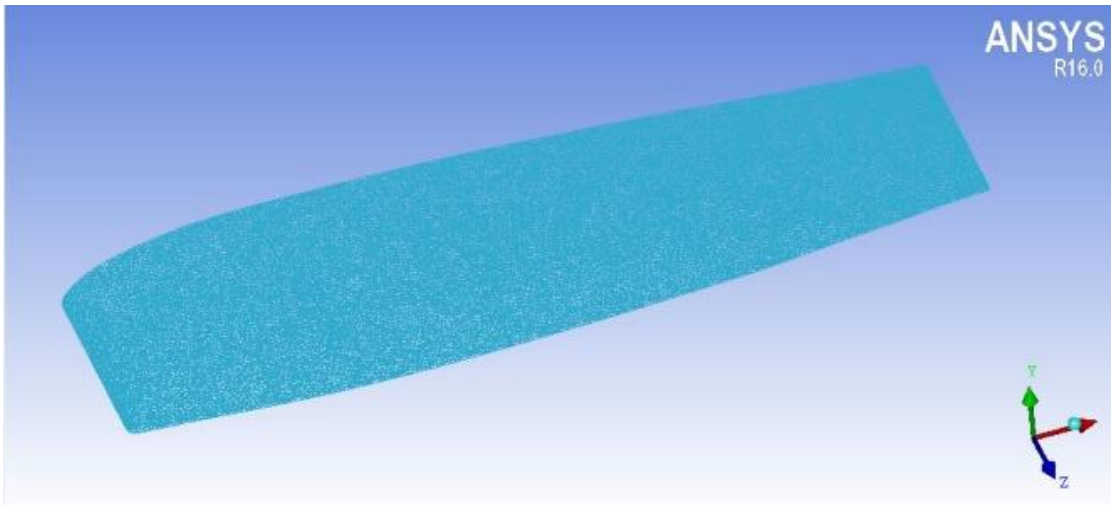

Figure 17 Surface mesh wireframe

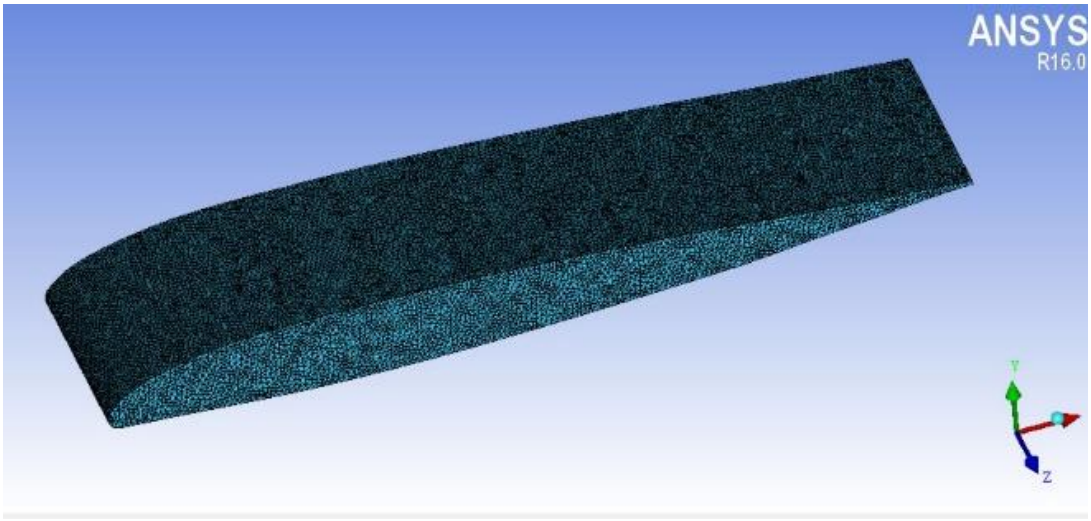

Figure 18 Surface mesh solid view

Finally, the surface mesh was generated then it was smoothed to get quality of 89 percent. Then general mesh sizes were given and volume mesh was generated using octree method. Finally, the domain having unstructured mesh of tetrahedral elements.

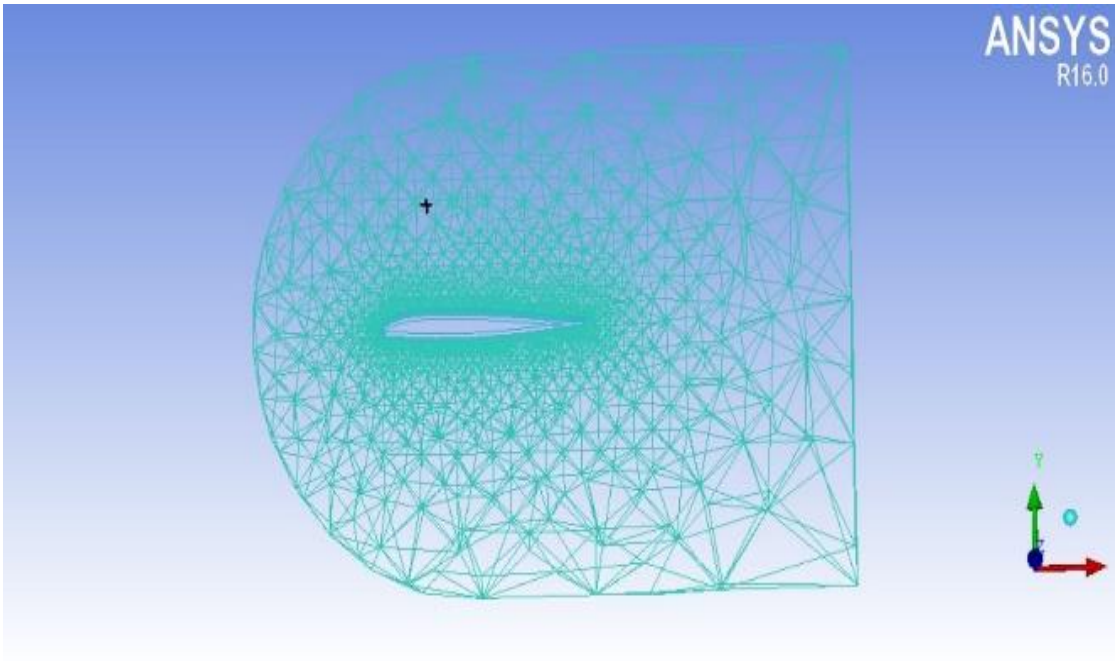

Figure 19 Volume mesh wireframe cut plane

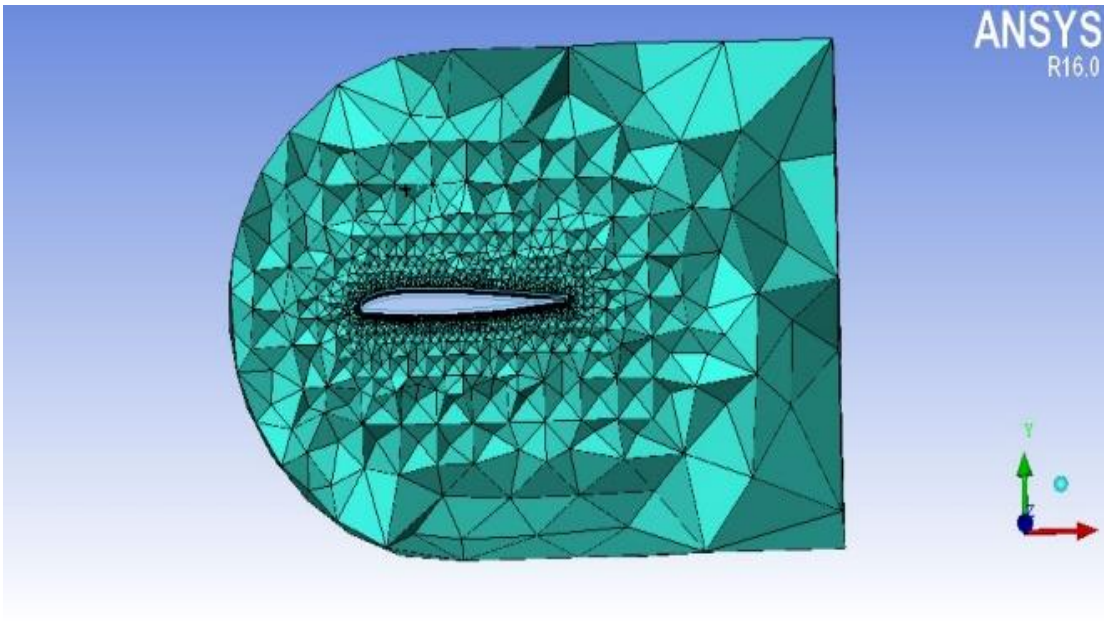

Figure 20 Volume mesh solid view cut plane

Then to correctly capture the effects of boundary layer prism layers were inserted using total layer thickness method. Y^+ selected was 30. Boundary layer height calculated using formula

Boundary layer calculation

First of all, Reynold number is calculated to check whether the flow is laminar or turbulent. Reynold number is calculated as

$$Re = \frac{\rho\, u\, L}{\mu}$$

Re = 1.22 * 66.67*1.35 / 1.793e-5

Re = 6.12e6

Reynold number greater than 500,000 shows the flow is turbulent. In order to calculate the turbulent boundary layer Blasius equation is used:

Boundary layer Thickness = $B.L = \frac{0.37\, x}{Re^{0.2}}$

= 0.37 * 1.35 / 6.12e6^.2

= 0.02 m

Boundary layer height came out to be 0.02m. Using total layer thickness 10 prism layers were inserted using exponential growth rate of 1.2 to capture the boundary layer.

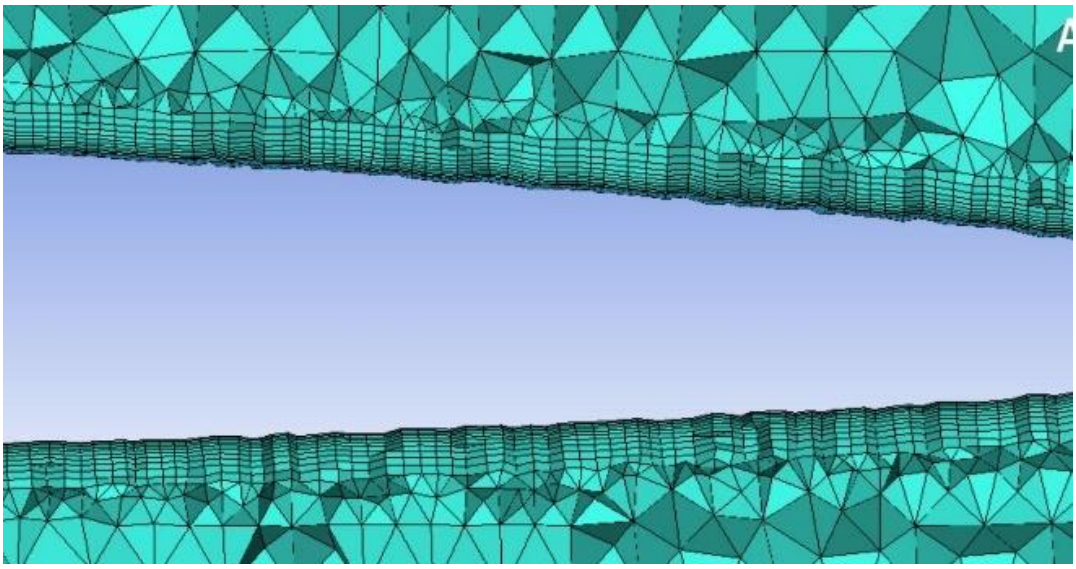

Figure 21 Prism layers

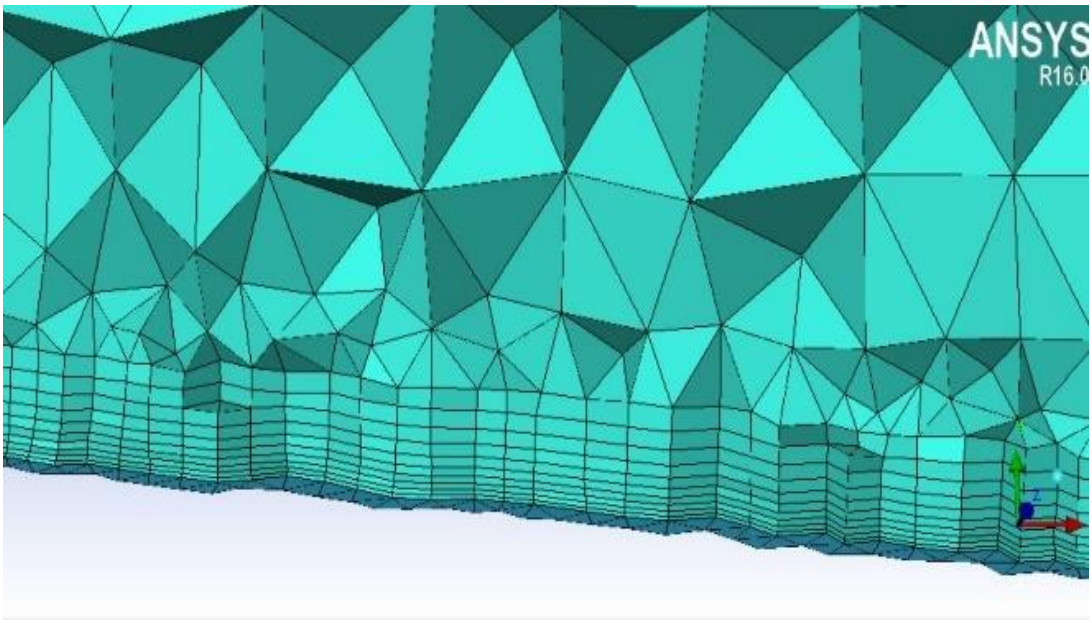

Figure 22 Prism layers closer view

Then using Laplace iterations volume, prism and tri mesh was smoothed having minimum orthogonal quality of 0.3 and quality of 87 percent.

Analysis

boundary conditions

velocity inlet was given with velocity of 67.7m/s in x direction. Domain walls top and bottom were also given as velocity inlet. Whereas wing was given boundary condition of wall with no slip condition having roughness height (Ks) of 0.0001. roughness height was given because the wing surface is not a smooth one and 0 roughness height indicates that its smooth wall.

setup

Turbulence model used is SST k-w with SIMPLEC(SIMPLE-Consistent) convergence scheme. SST k-w proved to have better results for adverse pressure gradient boundary layer.

Monitor for calculation of C_l and C_d were employed on wing surface to get values. Values of C_l and C_d were calculated and convergence criteria chosen was 1e-5. After 2300 iterations the residuals were stable to meet convergence criterion.

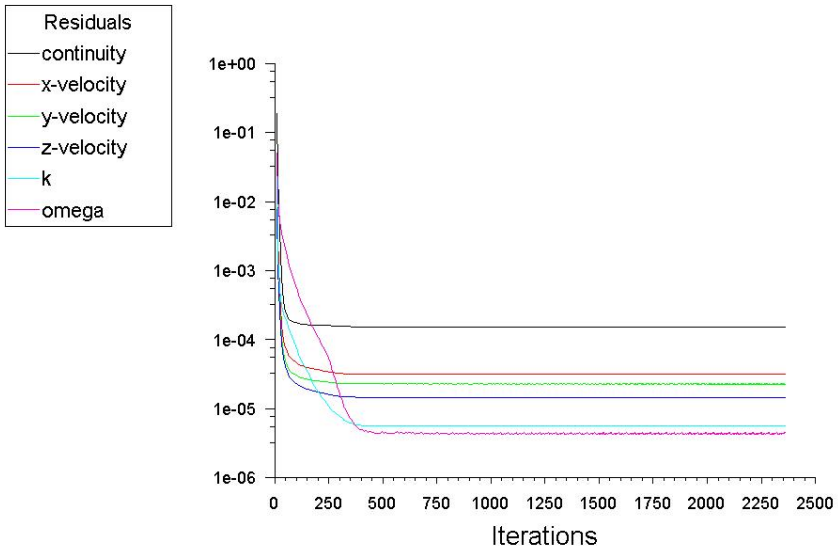

Figure 23 Convergence plot

The result of forces acting on wing are given below:

Forces result

Forces - Direction Vector (1 0 0)

Zone	Forces (n) Pressure	Viscous	Total
solid_1_1	12.217145	13.559982	25.777127
Net	12.217145	13.559982	25.777127

Figure 24 forces result on wing

As it can be seen viscous force magnitude is greater than magnitude of pressure force indicating that at 0 angle of attack viscous drag dominates the pressure drag as flow does not separates from wing, it remains attached to surface.

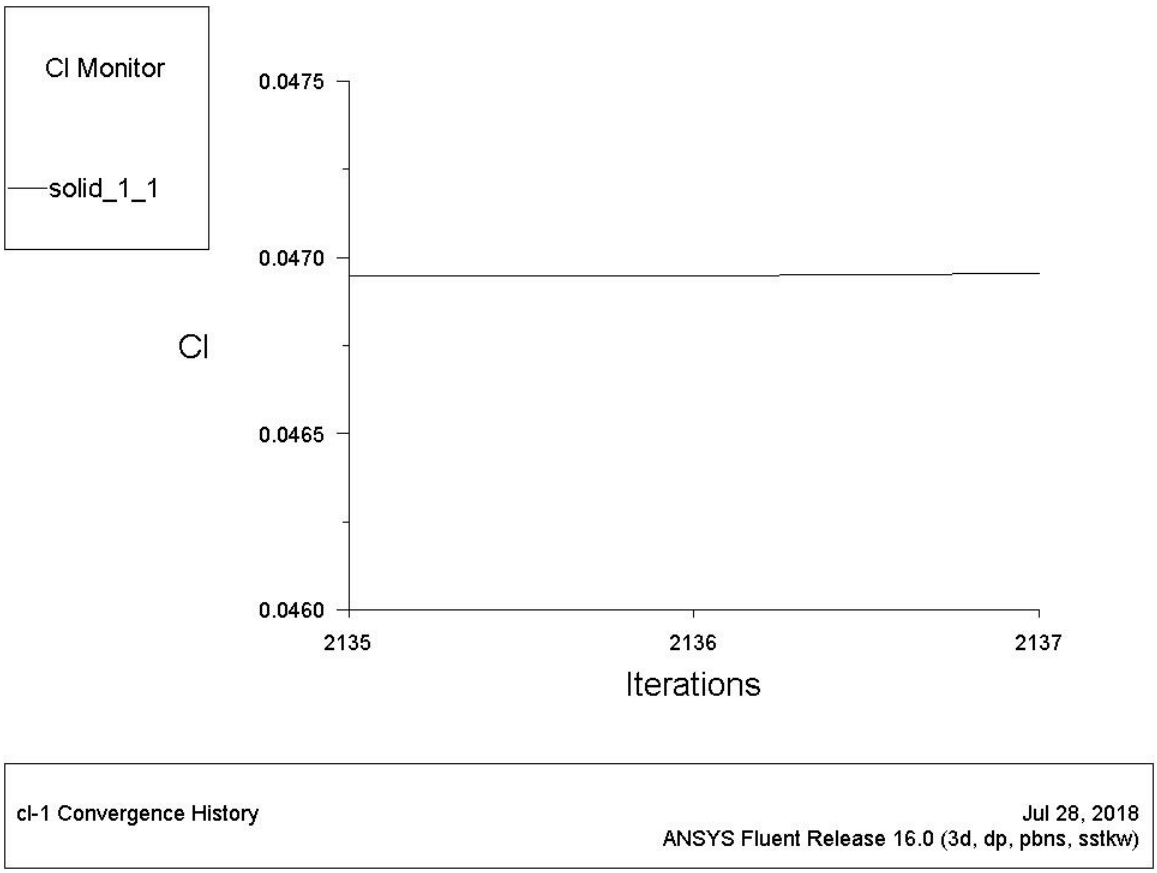

Figure 25 value of Cl

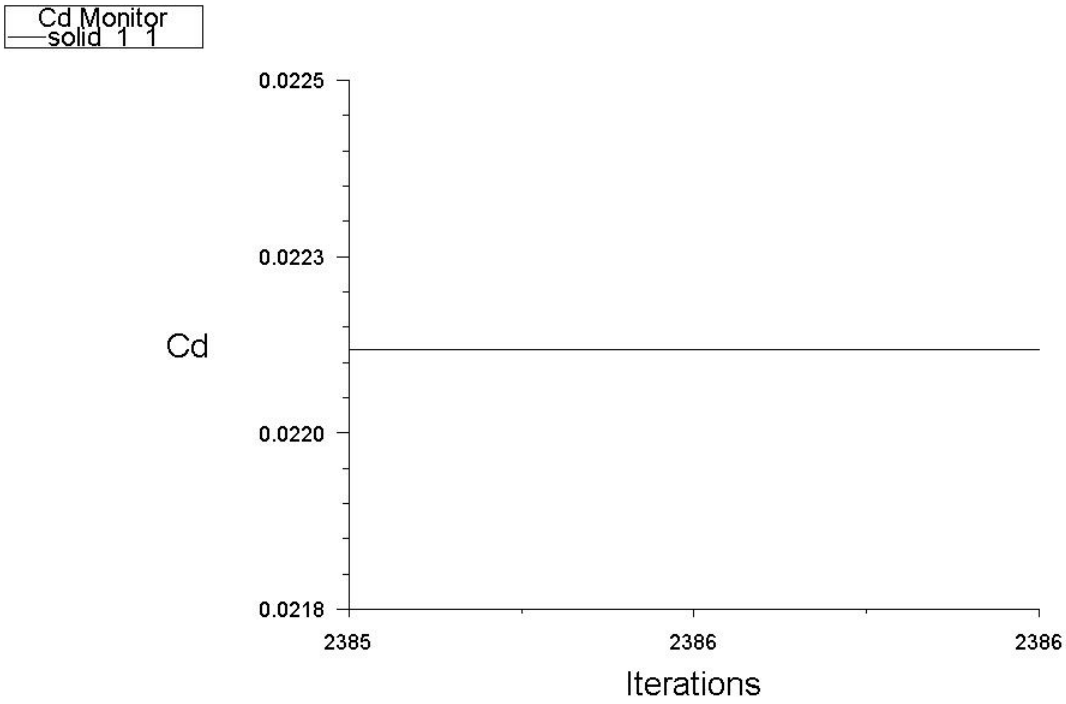

Figure 26 Value of C_d

Contours

Velocity contour was plotted to capture the flow physics. Boundary layer was perfectly captured showing that the velocity at surface of wing would be zero and would be increasing as the distance is increased away from wing. Flow physics shows the flow remains attached to surface as the analysis was done at zero angle of attack. It can be seen that there is no separation of flow thus viscous drag would be more as compared to pressure drag.

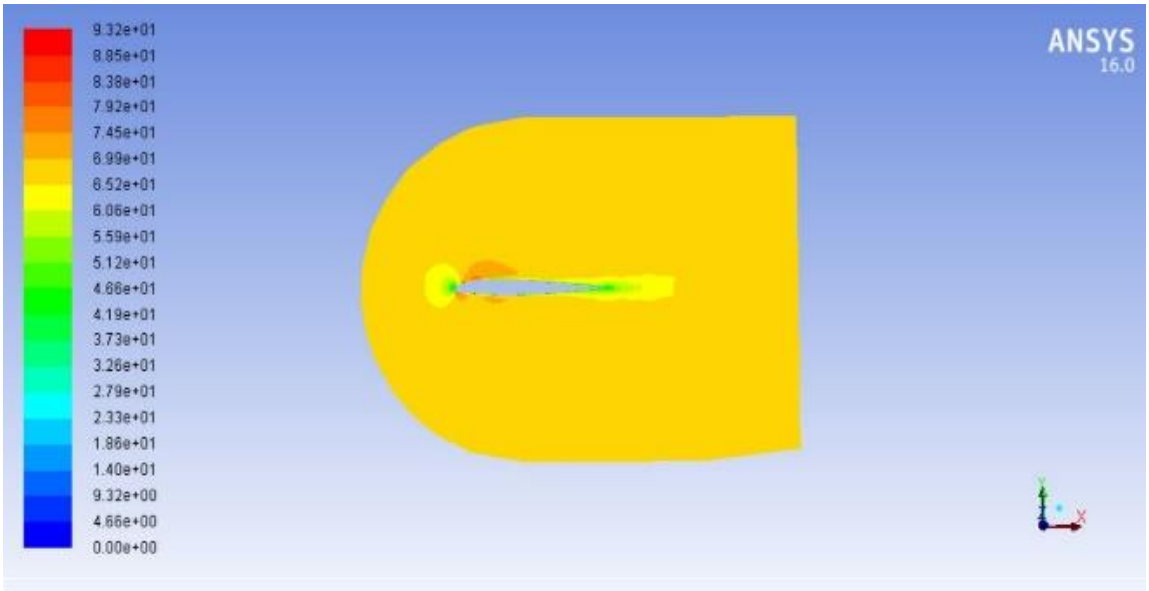

Figure 27 Velocity contour

4.2.2. RIVETED WING

Domain size was same as used in case of clean wing and remaining conditions were kept same to differentiate the drag difference in viscous as well as pressure drag in case of riveted wing. The domain used is shown as below:

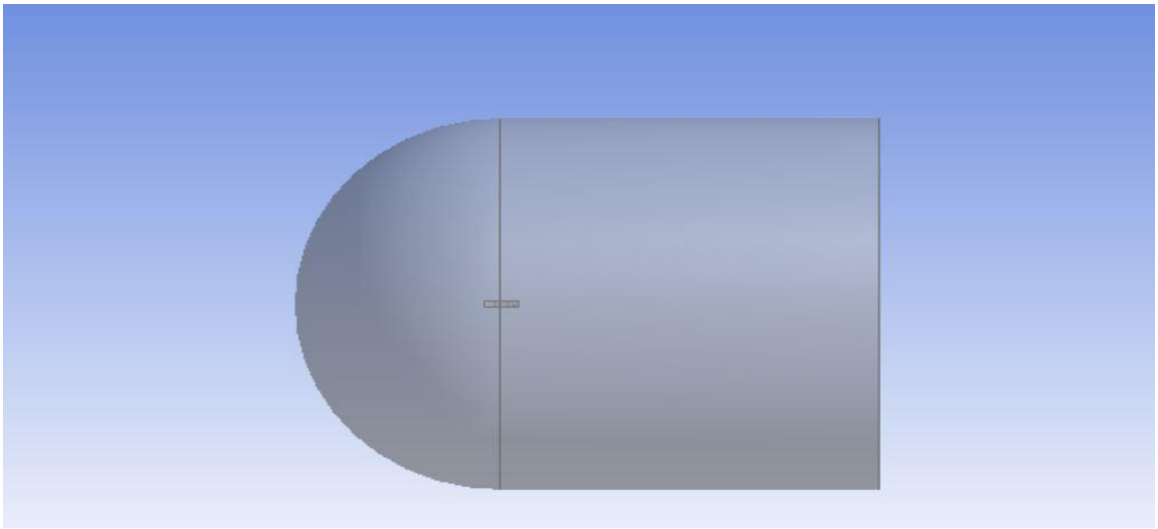

Figure 28 Riveted wing domain snip

Grid generation

ICEM CFD was used for generation of grid. Leading edge and trailing edge were given sizes of 1/512 whereas surface was given size of 1/256. In order to capture the rivets of 1mm they were given size of 1/1024. Then surface mesh was generated using patch independent method as it was not a perfectly smooth surface and triangular element was selected. Surface mesh was smoothed to make the quality better. Finally, the quality of surface mesh came out to be 82 percent.

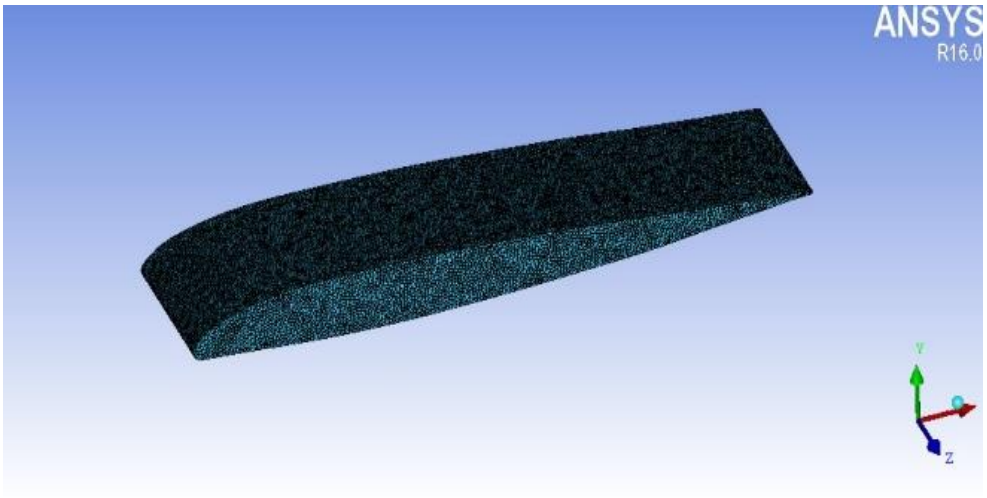

Figure 29 Surface mesh riveted wing

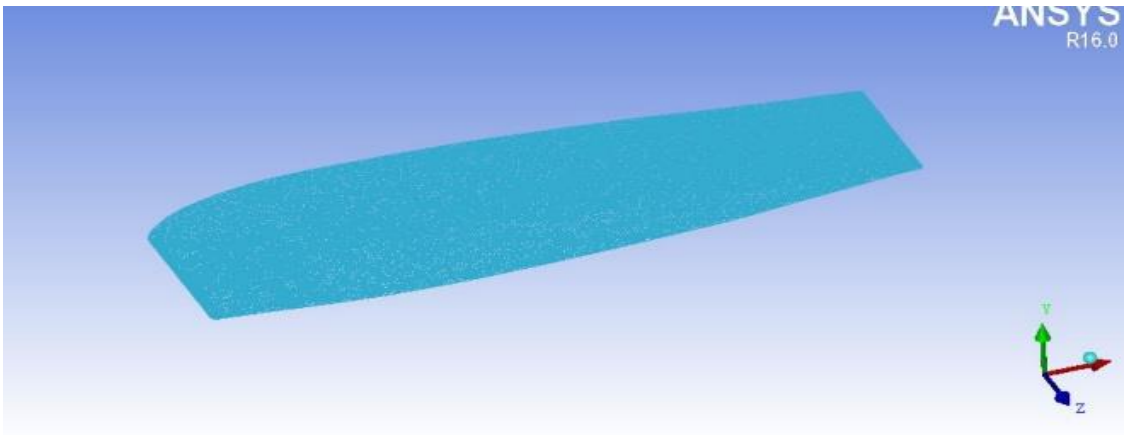

Figure 30 Surface mesh riveted wing wireframe

Using octree method volume mesh was generated consisting of tetrahedral elements.

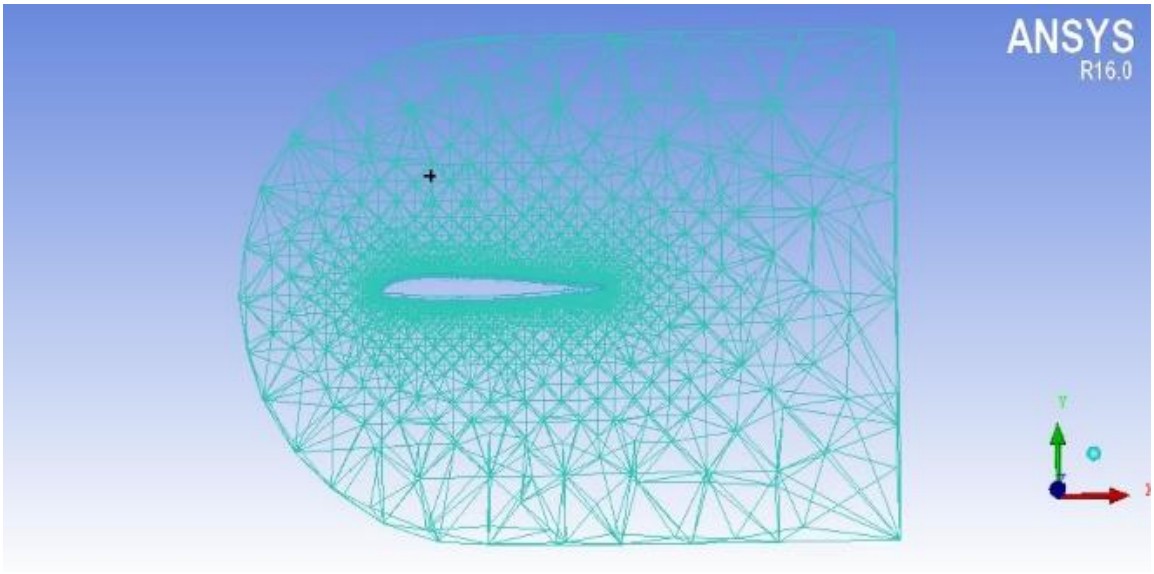

Figure 31 Volume mesh cut plane wireframe

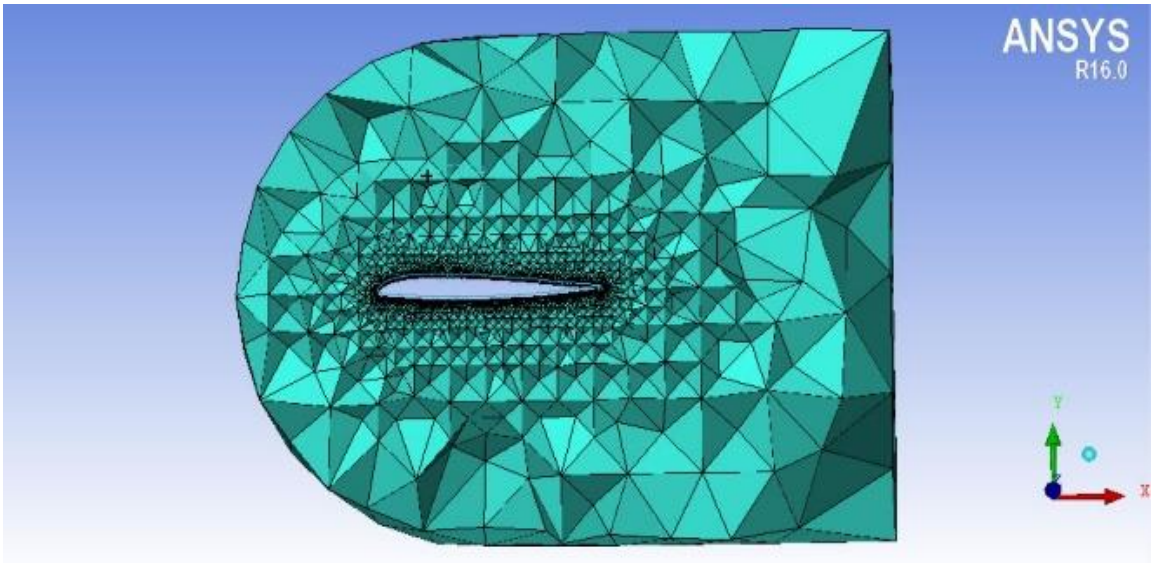

Figure 32 Volume mesh cut plane solid view

To capture boundary layer and effect of rivets inside boundary layer prism layers were used. Boundary layer was calculated but this time number of layers were 12 To capture the effects of rivet 15 layers were inserted with growth rate of 1.2 whereas height of first layer was fixed to be 0.000257m. Rivet height is 0.001m so first layer of prism mesh is catering the effect of rivet.

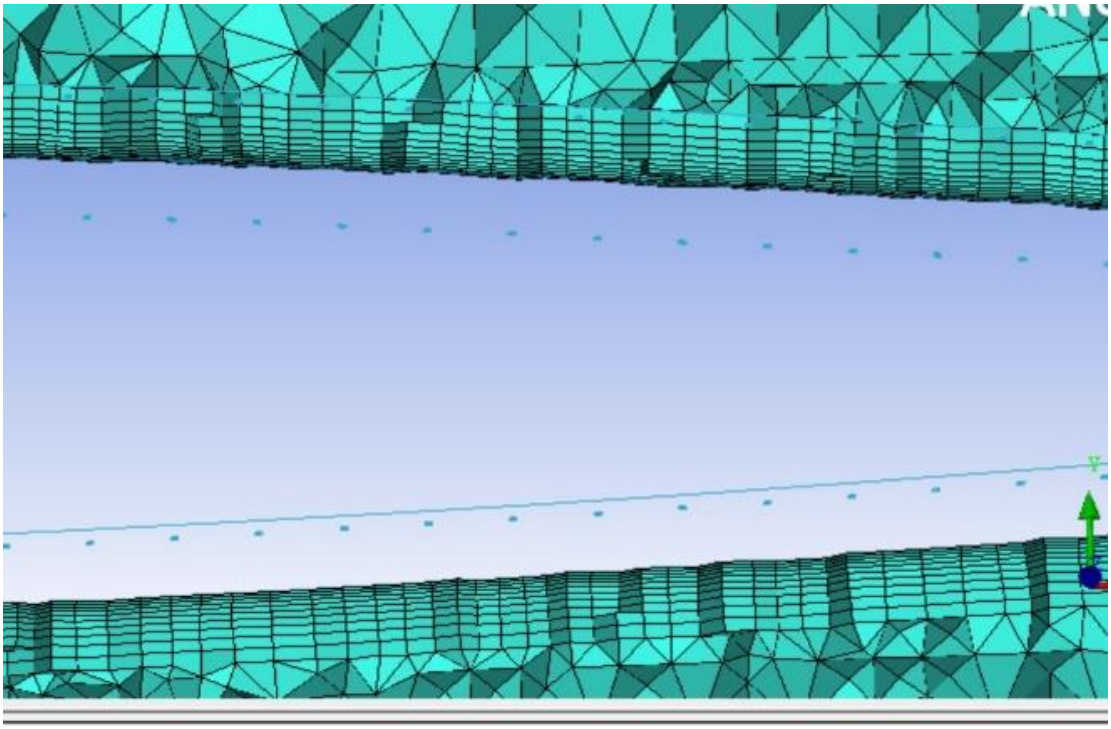

Figure 33 Prism layers in riveted wing

Then whole mesh consisting of tri, prism and tetrahedral elements was smoothed using Laplace iteration.

Analysis

SST k-w was employed to perform the analysis with SIMPLEC convergence scheme.

The value cd in this case is greater as compared to in case of clean wing whereas the value of cl decrease slightly. The convergence criteria used in this case was 1e-5. After 2100 the residuals became stable to meet the convergence criteria.

In this case viscous drag is more as compared to viscous drag in case of clean wing. This tangible increase is due to presence of rivets which falls inside the boundary layer and disturbs the flow making it turbulent.

Forces - Direction Vector (1 0 0)

	Forces (n)		
Zone	Pressure	Viscous	Total
solid_1_1	12.957467	14.020367	26.977834
Net	12.957467	14.020367	26.977834

Figure 34 Forces result on wing in riveted wing

C_d plot

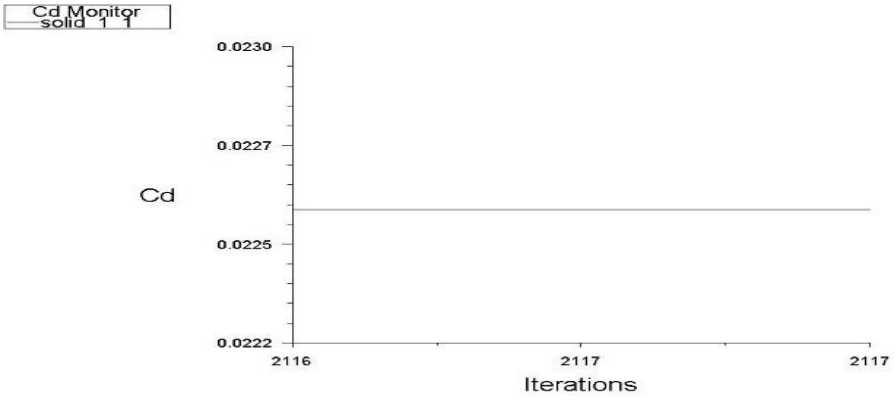

Figure 35 value of C_d

C_l plot

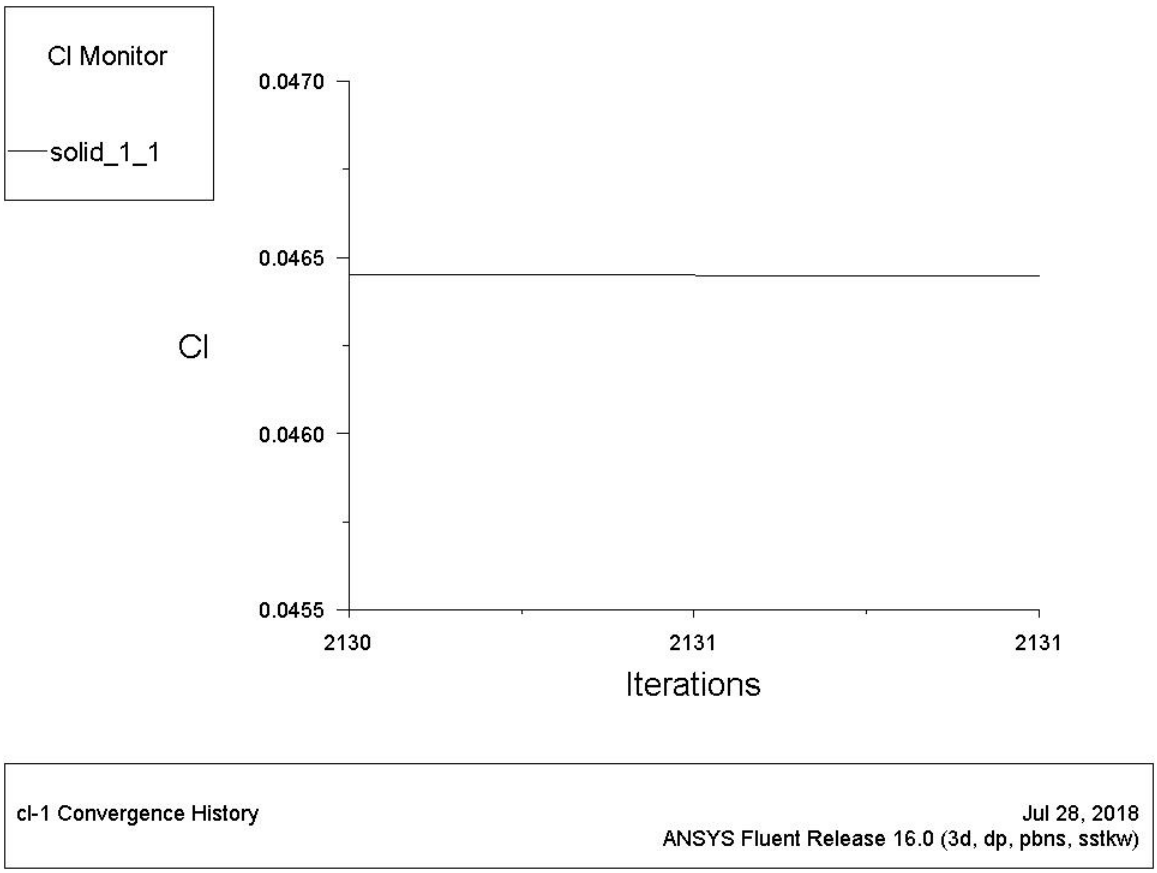

Figure 36 value of C_l

Contours

Velocity contours were plotted at different cut planes chord wise as well as span wise to observe the effects of rivets in disturbance of flow. Results indicate that at rivet point there is stagnation of flow making zero velocity and maximum pressure.

Chord wise plane

A dark blue color can clearly be seen indicating zero velocity in vicinity of rivet indicating that flow is stagnating at that point. The velocity increases as distance is increased away from surface.

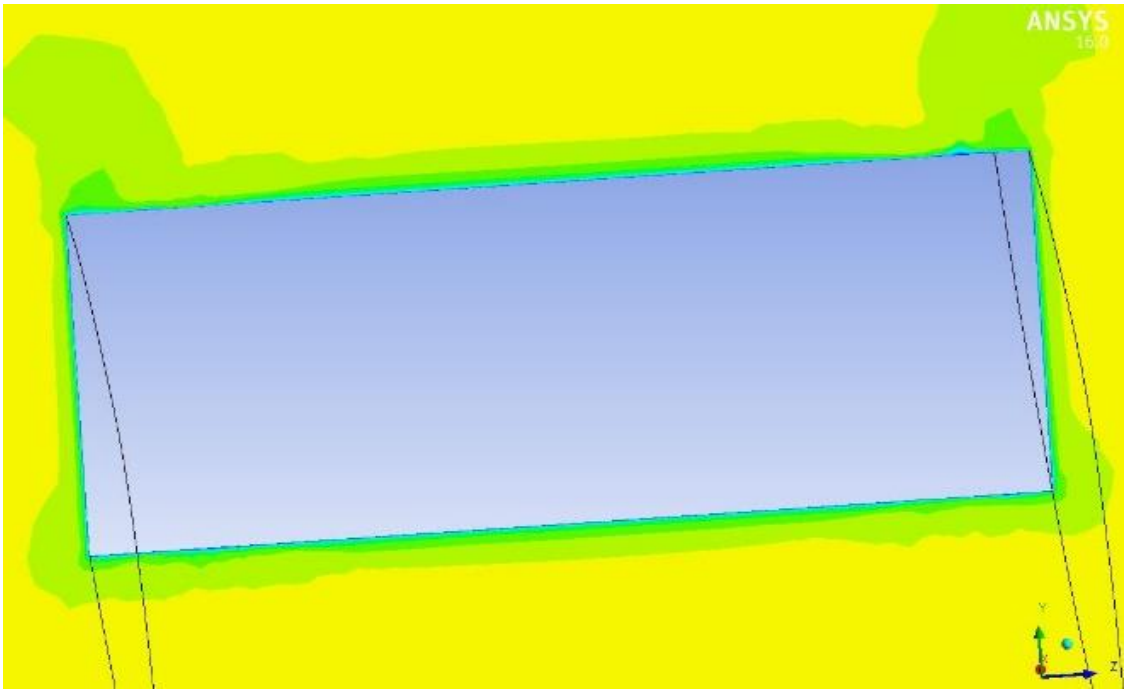

Figure 37 Velocity contour without rivets chord wise plane

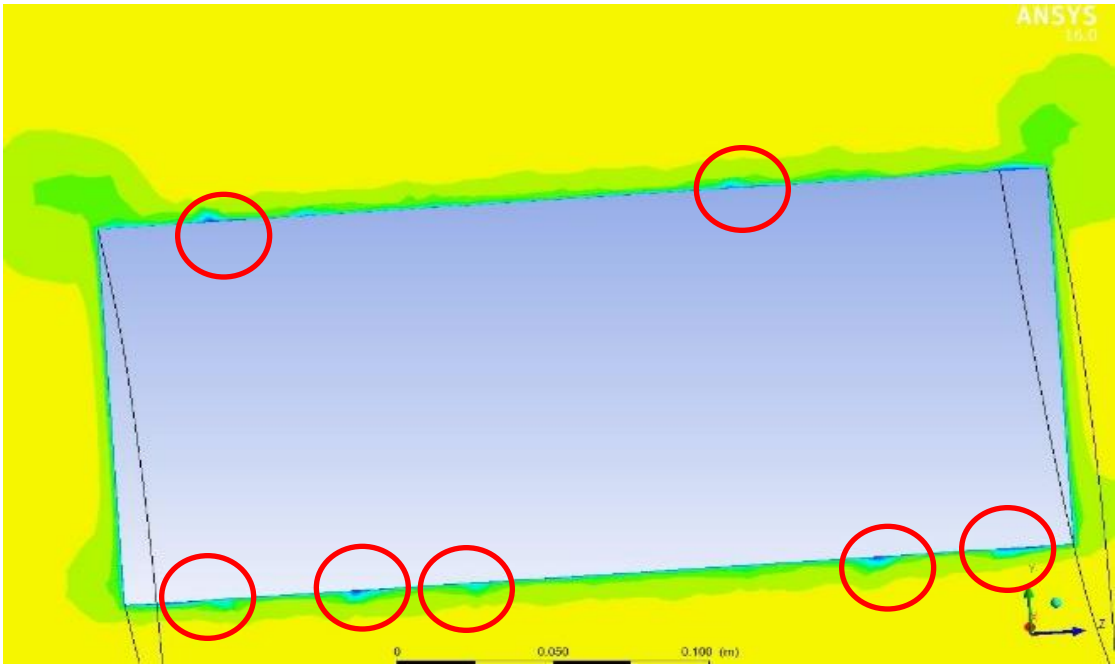

Figure 38 Velocity contour with rivets chord wise plane

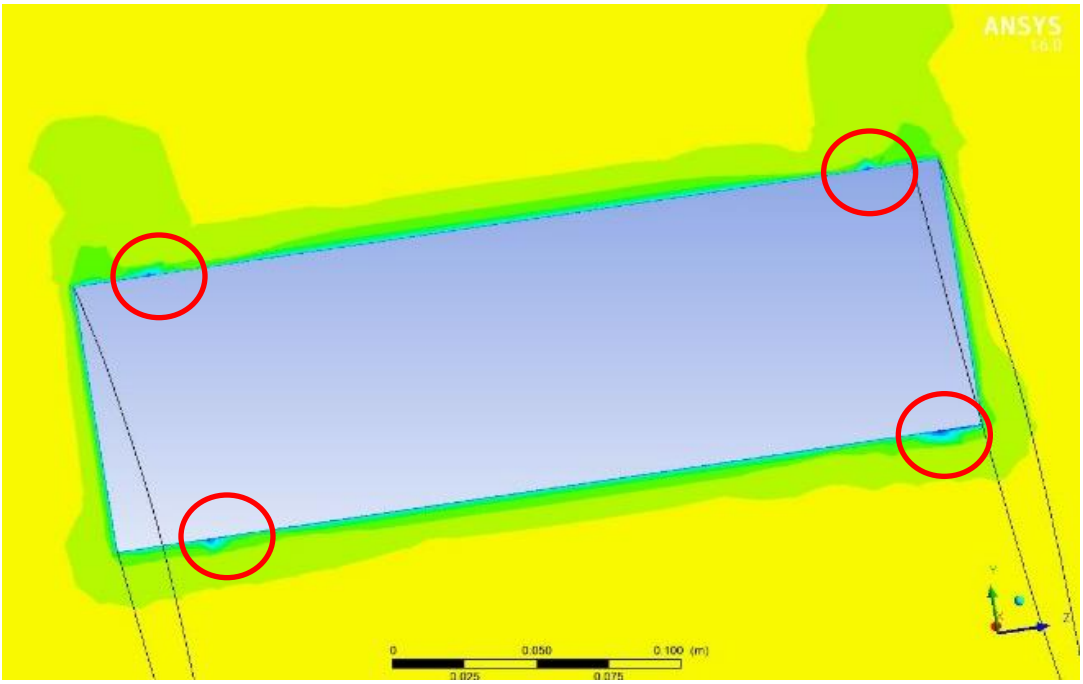

Figure 39 Velocity contour without rivets chord wise plane

Span wise plane

In case of riveted wing, it can be seen flow remains attached to wing due to presence of rivets. Pressure drag in this case is lower than viscous drag. Wake enlargement can also be observed comparative to clean wing wake.

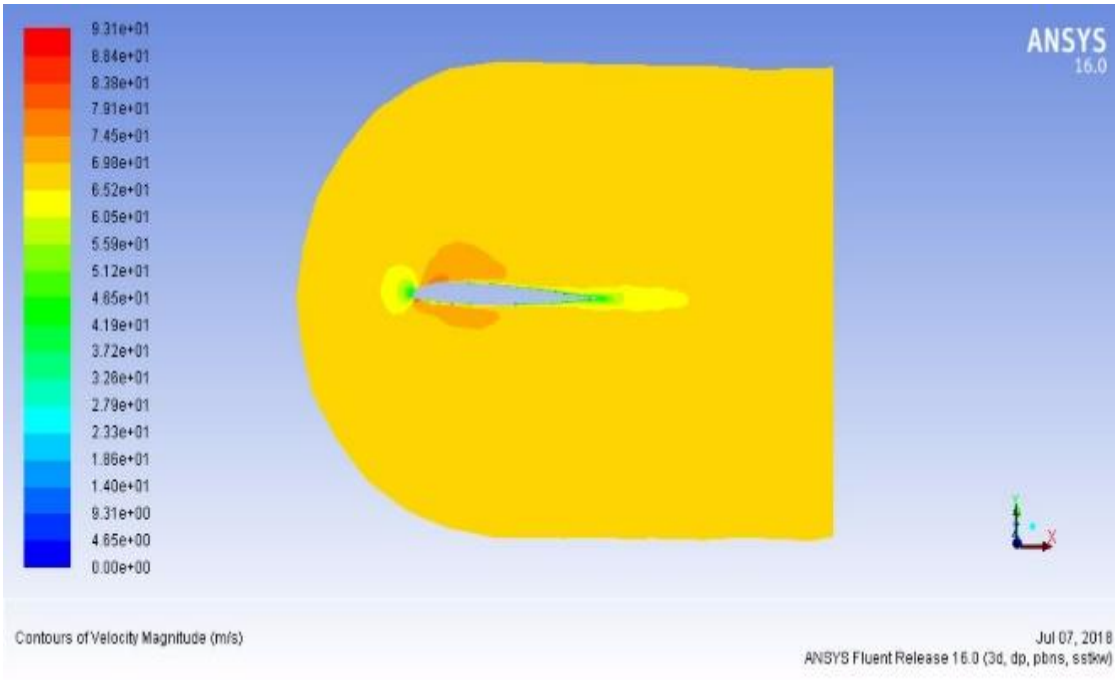

Figure 40 Velocity contour rivets span wise plane

Section plane cut where there are no rivets are present to observe the effect of rivets on wing. Then another section plane is cut having rivet to observe closely what is happening inside the vicinity of rivet.

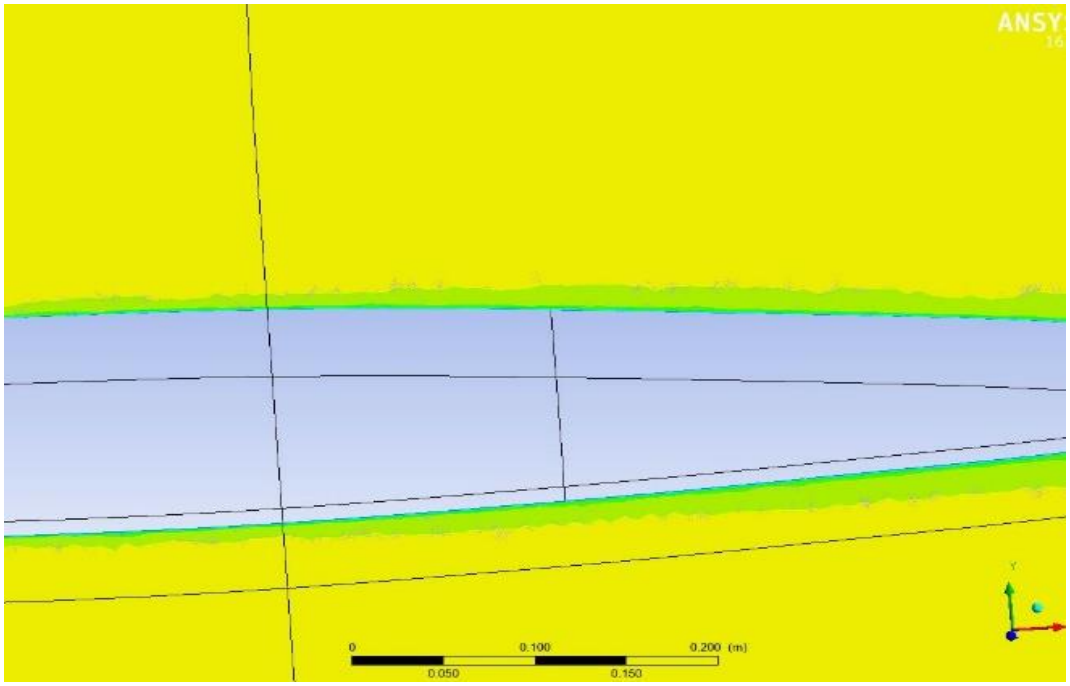

Figure 41 Velocity contour without rivets span wise plane

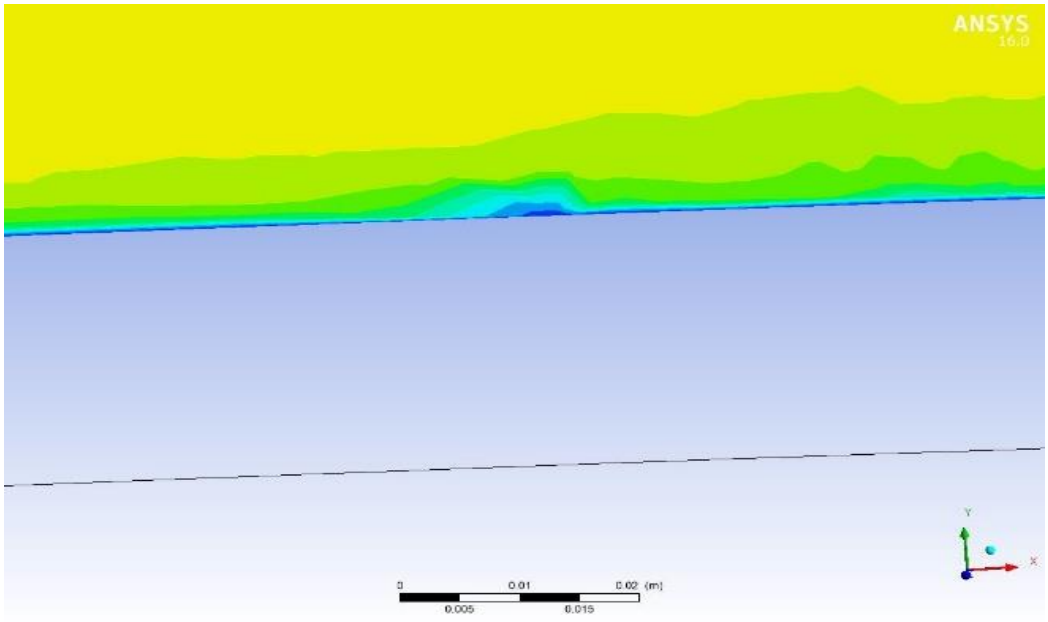

Figure 42 Velocity contour without rivets span wise plane closer view

4.2.3. Difference in results of clean wing and riveted wing

At zero angle of viscous drag must be more than pressure drag which can be seen in case of both clean wing as well as riveted wing but in case of riveted wing the viscous drag (14.0203) is more than clean wing(13.5599N) which is due to presence of rivets. Rivets are inside boundary layer hence they disturb the flow and force turbulent behavior. Pressure drag in case of clean wing is slightly more than riveted wing which is due to separation. Rivets increase the viscous drag keeps the flow attached to wing whereas in case of clean wing flow separates. The attachment of flow can be observed in velocity contour of riveted wing or it may be called as wake enlargement. Presence of rivets increase the drag.

Drag difference = riveted wing drag – clean wing drag

= 26.977834 – 25.777127

=1.20N

4.2.4. Different angles of attack

Further the analysis of riveted wing was performed at increasing angle of attack to observe the difference in pressure drag as compared to viscous drag. Pressure drag must be more than viscous drag as at higher angle of attack the flow must separates increasing the pressure drag. Angles selected for analysis are -5, 5, 10 degrees. The results would be tabulated to observe the difference.

-5 degrees

The direction of flow was specified in fluent. Geometry and mesh settings were kept constant.

For flow direction the flow was broken down into components. F represents flow. L represents lift. D represents drag.

F = cos 5 - sin 5

L = sin 5 + cos5

D =-cos 5 + sin 5

Then values of Cl, Cd and forces results are as follows;

C_d plot

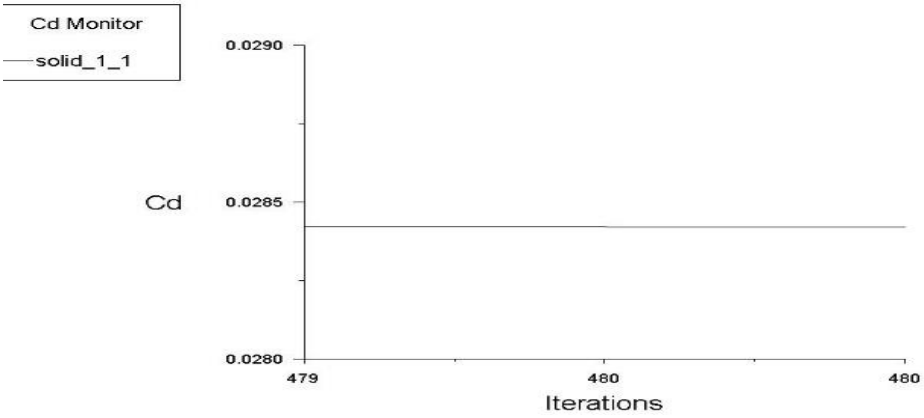

Figure 43 value of C_d in -5 degrees

Forces result

Forces (n)

Zone	Pressure	Viscous	Total
solid_1_1	22.509357	10.522341	33.031698
Net	22.509357	10.522341	33.031698

Figure 44 Forces result at -5 degrees

Velocity contour

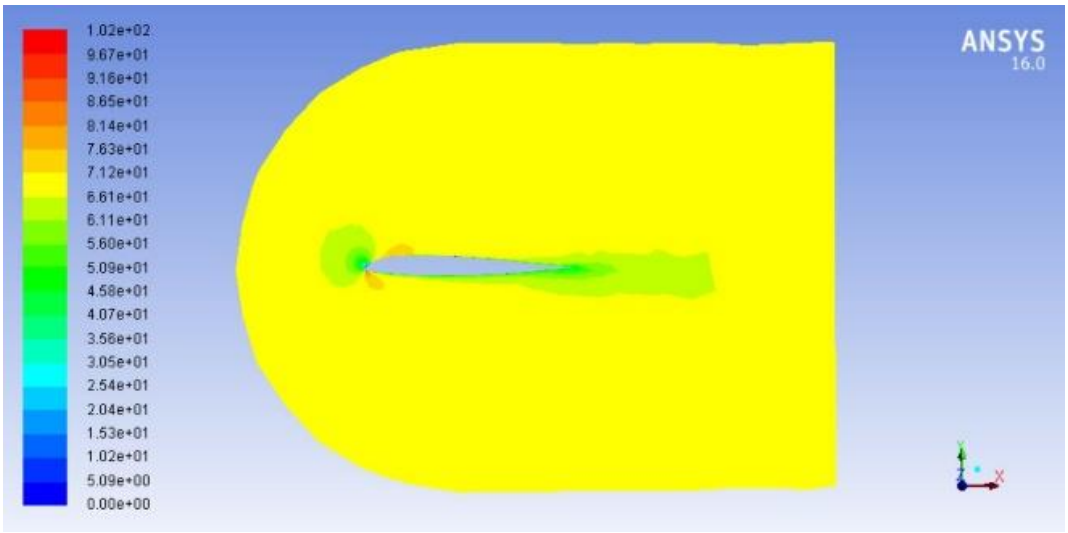

Figure 45 Velocity contour at -5 degrees

From forces results it can be deduced that pressure drag is more as compared to viscous drag and velocity contour indicating that flow is getting separated. Wake of flow is showing separation from bottom of wing due to direction of flow.

5 degrees

For 5 degree the components of flow are as;

F = cos 5 + sin 5

L = -sin 5 + cos5

D =-cos 5 – sin 5

Forces result

Forces - Direction Vector (1 0 0)

Zone	Forces (n) Pressure	Viscous	Total
solid_1_1	18.378528	11.389932	29.76846
Net	18.378528	11.389932	29.76846

Figure 46 Forces value at 5 degrees

C_d plot

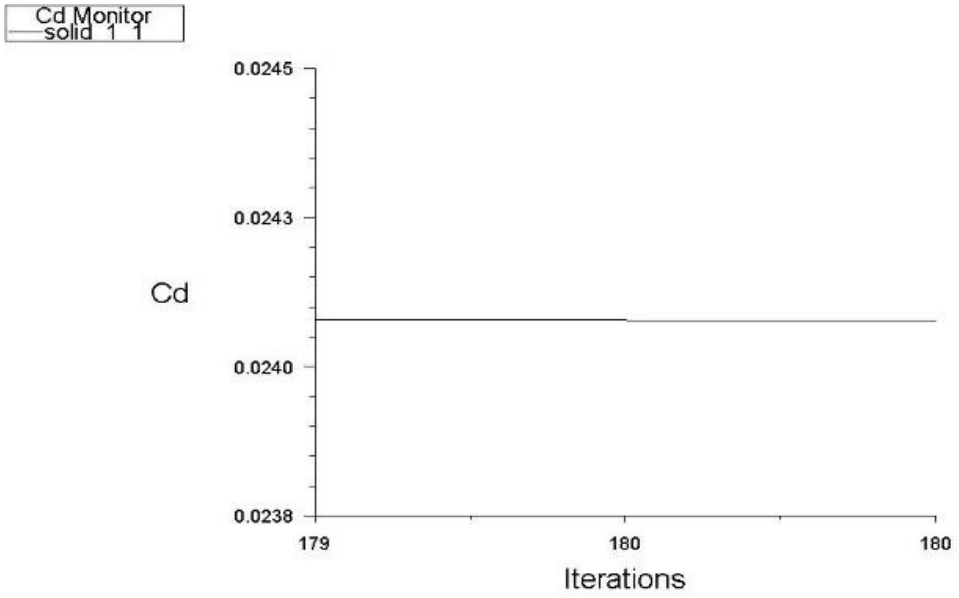

Figure 47 value of C_d at 5 degrees

Velocity contour

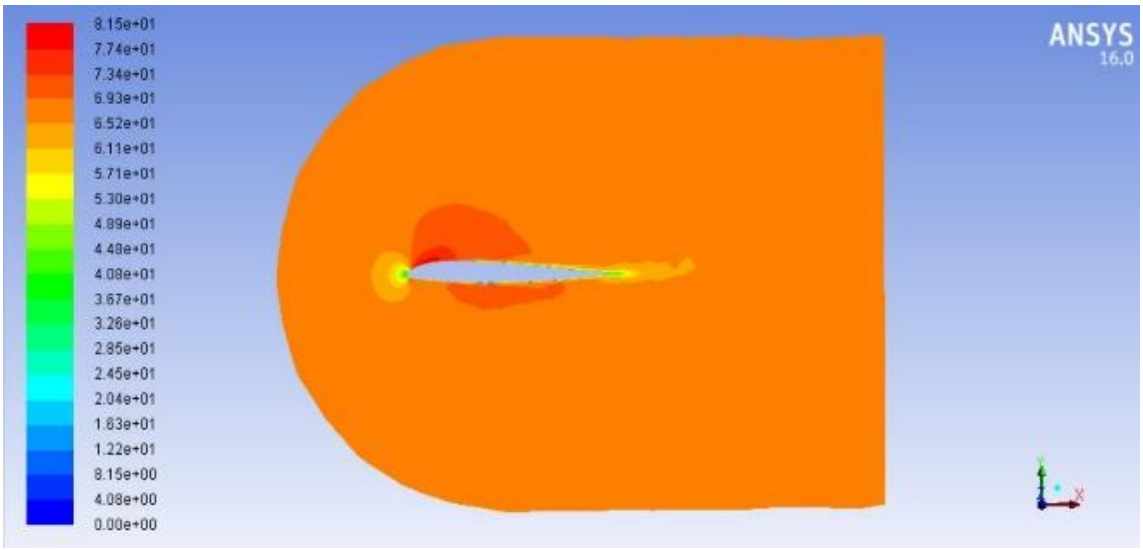

Figure 48 Velocity contour at 5 degrees

Results indicate that at 5 degrees angle of attack the C_d is more as compared to wing at zero angle of attack. Pressure drag is more as compared to viscous drag indicating the separation of flow.

10 degrees

The direction of flow in components here is

F = cos 10 + sin 10

L = -sin 10 + cos 10

D =-cos 10 – sin 10

Forces result

Forces - Direction Vector (1 0 0)

Zone	Forces (n) Pressure	Viscous	Total
solid_1_1	25.206752	10.733356	35.940108
Net	25.206752	10.733356	35.940108

Figure 49 Forces result 10 degrees

C_d plot

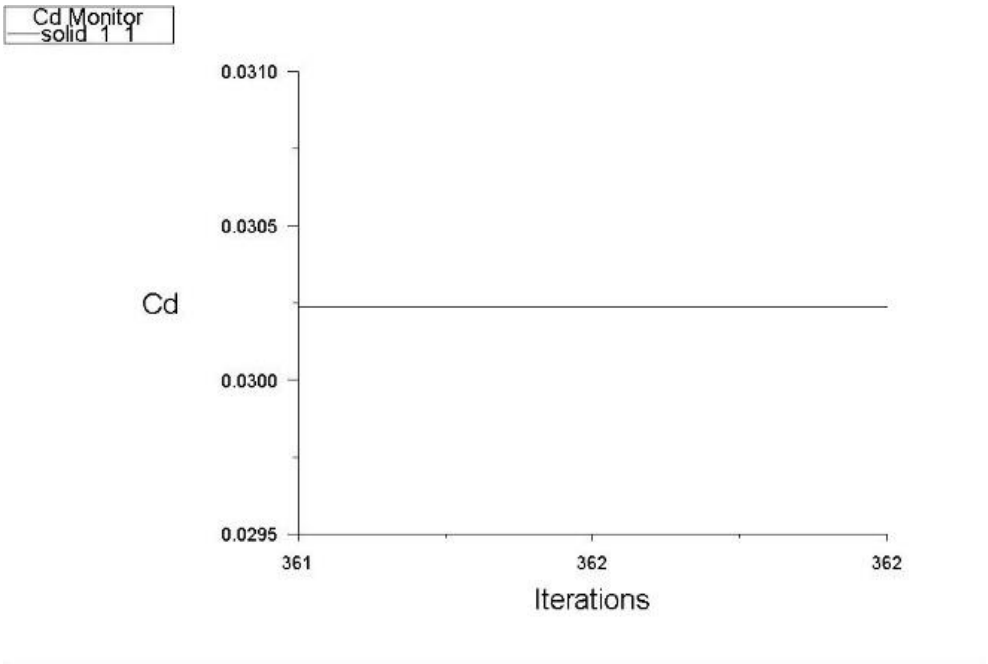

Figure 50 C_d value at 10 degrees

Velocity contour

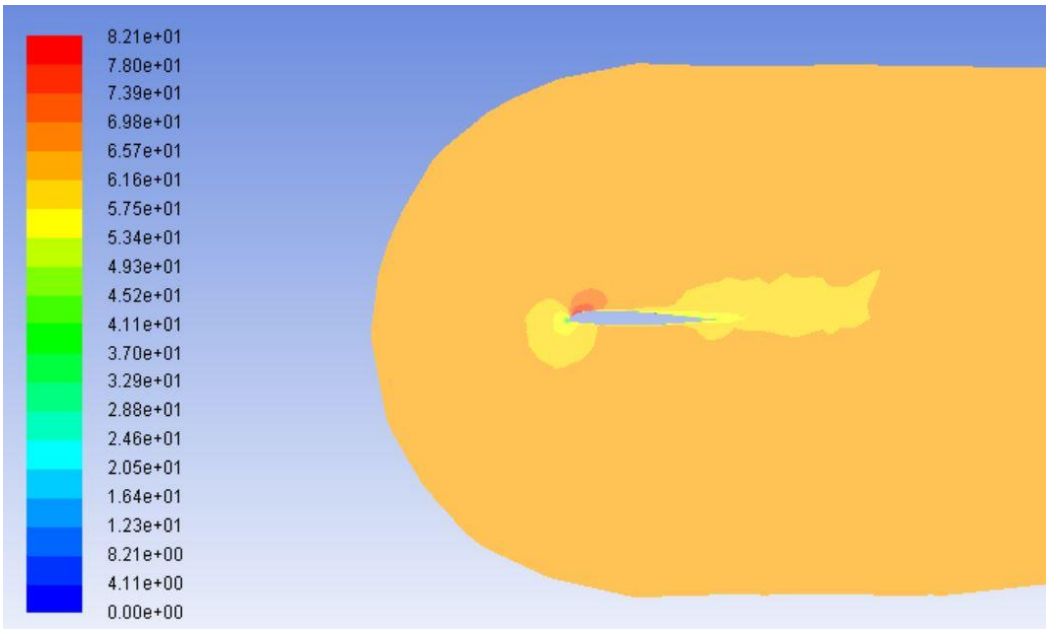

Figure 51 Velocity contour at 10 degrees

In case of wing at 10 degrees of angle of attack pressure drag is more than twice of viscous drag. Flow separation is clearly evident from velocity contour. As it can be seen that flow gets separated from to side of wing due to wing at being positive angle of attack.

4.3. Analytic validation

Component buildup method

This method estimates the subsonic parasite drag of each component of aircraft using skin friction drag coefficient and form factor that evaluates the pressure drag that occurs due to separation of flow [2]. In this case as the wing is under consideration so this method will be implemented for wing that presents the crude estimation of drag acting on wing to validate the results of CFD.

For laminar skin friction drag formula used is

$$C_f = \frac{1.328}{\sqrt{R_e}}$$

And after 0.3 chord the flow is turbulent for which skin friction drag is calculated using

$$C_f = \frac{0.455}{(log_{10}R)^{2.58}}$$

R is Reynold cut off which is calculated using

$$R_{cut\ off=}38.21(\frac{l}{k})^{1.053}$$

Value of k (skin roughness) for smooth paint is2.08e-5 ft.

Form factor to calculate pressure drag is calculated using this formula

$$FF = 1 + \frac{0.6}{(X/c)m}\left(\frac{t}{c}\right) + 100\frac{t^4}{c}$$

Drag calculated using this formula

$$\underline{C_D} = \frac{C_{fc}FF_cQ_cS_{wet_c}}{S_{ref_c}}$$

Parameters

Surface area of wing are calculated using CATIA model used.

Clean wing total surface area = upper surface + lower surface + leading edge + trailing edge

= 1.1134 m^2

One rivet surface area = 0.034465 cm^2

334 rivets surface area = 334 * 0.034465

=0.001151 m^2

Riveted wing total surface area = 1.1134 + 0.001151

= 1.114551 m^2

Reference area = 0.4185 m^2

Maximum thickness = 0.13m

Mean aerodynamic chord = 1.35m

t/c (max thickness to chord) =0.09629

x/c (location of max thickness to chord) = 0.3

Result

Using this equation and substituting values

$$C_D = \frac{C_{fc} FF_c Q_c S_{wet_c}}{S_{ref_c}}$$

Cf_c = 0.006076

FF_c = 1.20

Q_c = 1

S_{wet} = 1.1134 m^2

S_{ref} = 0.4185 m^2

after putting all the values, the C_d was calculated for clean wing then surface area of rivets was added and C_d value for riveted wing was calculated.

Value of C_d for clean wing = 0.0193979

Total Drag acting on clean wing = 0.0193979 * 1134.71

=22.011 N

Value of C_d for riveted wing = 0.0194179

Value of C_d for clean wing = 0.0194719 * 1134.71

= 22.0536 N

Difference in drag between clean wing and riveted wing = 22.0536 – 22.011

= 0.0426 N

4.4. Validation via earlier work

Wind tunnel testing of scale down model of aircraft was carried out by earlier at zero angle of attack in which the total drag acting on aircraft was 3871N.

Using component build up method reverse approach and historic trends.

Drag acting on wing	=	15-20 % of total drag
Drag acting on fuselage	=	30-35 % of total drag
Drag acting on horizontal tail	=	5-7 % of total drag
Drag acting on vertical tail	=	3-5 % of total drag
Miscellaneous drag including all other	=	30-40 % of total drag

In this way, drag acting on wing assumed to be 17% of total drag. Thus,

= 0.175 * 3871

= 677.425 N

As selected span is 0.31m which 1/28 of original span(8.85m). so,

Drag on 0.31m span = 677.425 / 28

= 24.2 N

5. DISCUSSION AND ANALYSIS

Previously the CFD of the whole aircraft has been done without catering the effects of rivets on drag. So, the analysis was carried out to observe how much drag is caused due to presence of rivets on wing. After the analysis it is cleared that presence of rivets not only keep the flow attached to surface of wing but also results in greater viscous drag. Results of whole analysis are presented in tabulated form:

Clean wing

angle	Cl	Cd	Pressure drag	Viscous drag	Total drag
0	0.0047	0.0220	12.21	13.55	25.77

Riveted wing

angle	Cl	Cd	Pressure drag	Viscous drag	Total drag
-5	0.01974	0.0284	22.5	10.52	33.03
0	0.0465	0.0226	12.95	14.02	26.97
5	0.194	0.0240	18.37	11.38	29.76
10	1.01	0.0303	25.2	10.733	35.94
15	0.260	0.0760	78.17	9.98	88.15

Graph of Cl and Cd vs alpha

From this analysis it is evident when angle of attack is increased Cl also increased which is in accordance with normal trend of Cl with increasing angle of attack.

Graph 1 Cl-alpha

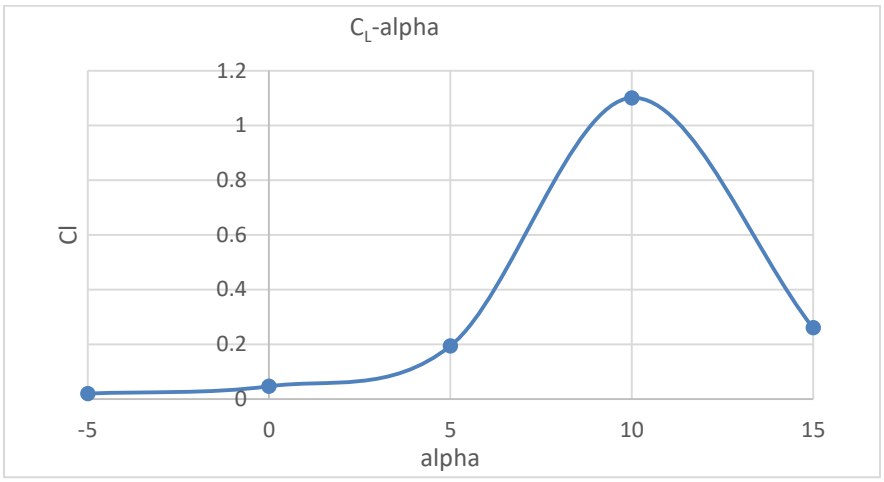

Similar behavior can be seen in case of Cd with increasing angle of attack.

Graph 2 Cd-alpha

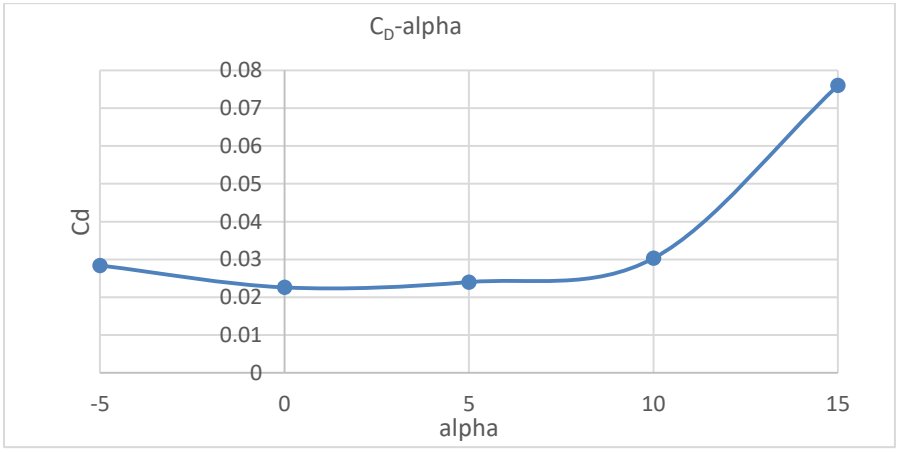

Graph of viscous and pressure with alpha

It can be seen with increasing angle of attack the pressure drag increases. The reason is with increasing angle of attack the flow separates from surface of wing hence viscous drag can be seen exhibiting decreasing trend with respect to increasing angle of attack. At zero angle or cruise angle of attack viscous drag dominates pressure drag as there is no separation of flow.

Graph 3 viscous drag vs alpha

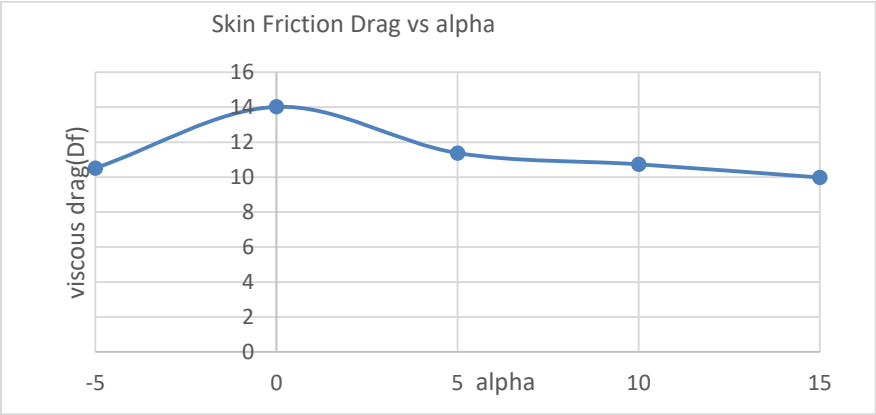

Graph 4 pressure drag vs alpha

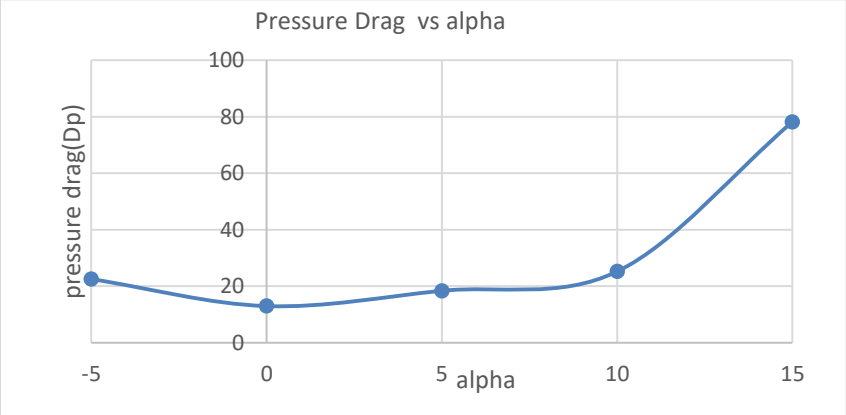

6. RECOMMENDATIONS

if computational power is available whole model of aircraft with rivets modelled on it can be analysed provided value of y+ to be as small as possible to cater the rivets and their effect in boundary layer region. This would provide exact solution rather than estimations done due to lack of computational power. The turbulent flow in boundary layer region can be studied in detail. Effect of disturbance caused due to rivets presence can be observed. Moreover, wing of 0.31m span be fabricated which was done due to administrative problems and lack of time to validate the results exactly with wind tunnel testing.

Exact wing of span 0.31m and mean aerodynamic chord of 1.35m can be fabricated to study the effect of rivets on wing in wind tunnel to experimentally validate the results which could not be done due to administrative reasons.

7. CONCLUSION

Aerodynamic shape of aircraft is important parameter in describing the forces acting on aircraft. Blunt shape would cause greater pressure drag. Rough surfaces will cause the increased skin friction drag. When designing an aircraft, the shape of aircraft is considered as utmost parameter.

1. Countersunk flush rivet is an effective solution for this problem.
2. Sheet with some adhesive material can be spread over aircraft that smoothed the aircraft surface and reduce the effect of any protruding surface to flow over aircraft.

Following conclusions can be drawn by the results of CFD

1. The value of C_d decreases from 0.0226 to 0.0220 by countersunk all the rivets thereby increasing the L/D from 2.205 to 2.136.
2. The value of C_l increases from 0.0465 to 0.047 by countersunk all the rivets hence giving an increase of 1.0638% in C_l.
3. Range can be increased by 4.2%. Range of considered aircraft is 814km. by countersunk all rivets it can be increased by 34 km making total range of 848km at cruise condition.
4. Fuel consumption at economy cruise setting for 155hp is 12 gallons/hr. 0.049 gallons of 100LL gasoline can be saved per sortie at economy cruise setting which save 0.1638$/sortie.

8. REFERENCES

[1] M. C. a. V. C. S. Fischer, "Application of laminar flow control to the high speed civil transport the NASA supersonic laminar ¯ow control program," *SAE paper 91-2115, ,* 1991.

[2] D. P. Raymer, Aircraft Design: A Conceptual Approach 2ndEdition, 1989.

[3] S. J., "Viscous drag reduction on transport aircraft," *AIAA paper 910685,* 1991.

[4] J. a. R. J. O. Priest, "Recent developments in international laminar flow research programs for transport aircraft.," *TP P-1992-163, ,* 1992 .

[5] D. M. a. H. J. N. Bushnell, "Viscous Drag Reduction in Boundary Layers," *AIAA Progress in Astronautics and Aeronautics, (American Institute of Aeronautics and Astronautics),* vol. Vol. 123, 1990.

[6] J. A. D. a. C. E. Cousteix, "Reduction of aerodynamic skin friction drag.," *Nouvelle Revue d'Aeronautique et d'Astronautique, ,* April 1993.

[7] C. H. C. D. C. a. K. G. E. Crawford, "Laminar and turbulent ¯ow over optimal riblets.," in *In Proceedings of the '92 European Computational Fluid Dynamics Conference*, Brussels, Belgium,, 7±11 September 1992.

[8] D. M. Bushnell, "Fluid mechanics, drag reduction, and advanced coneguration aeronautics.," *NASA TM-2000- 210646, ,* 2000..

[9] J. M. C. A. a. C. C. Janus, "Computational analysis of methods for reduction of induced drag," *AIAA paper 93-0524,* 1993..

[10] M. D. Oser, "Eliminating and separation and reducing viscous drag through boundary layer analysis and manipulation.," *Langley Aerospace Research Summer Scholars, 1995, pp. 555±563, paper N97-11867.*, 1995.

[11] J. D. Anderson, Fundamentals of Aerodynamics, Boston: McGraw-Hill, 2001.

[12] D. Wilcox, "Turbulence Modeling for CFD," *DCW Industries, Inc., La Canada, CA, ,* 1993.

[13] D. C. Wilcox, "Comparison of Two-Equation Turbulence Models for Boundary Layers with Pressure Gradient,," *AIAA Journal,* vol. Vol. 31, no. No. 8, pp. pp. 1414-1421, 1993.

[14] B. a. S. R. Abu-Ghannam, "Natural Transition of Boundary Layers-The Effects of Turbulence, Pressure Gradient, and Flow History," *Journal of Mechanical Engineering Science,* vol. Vol. 22, no. No. 5, p. pp. 213 – 228., 1980.

[15] A. a. L. S. Hellsten, "Extension of the k-w-SST turbulence models for flows over rough surfaces," *AIAA Paper 97-3577,* 1997.

[16] E. R. a. B. C. B. Van Driest, "Boundary Layer Transition: Freestream Turbulence and Pressure Gradient Effects," *AIAA Journal,* vol. Vol. 1, no. No. 6, p. pp. 1303–1306., June 1963.

[17] "National Advisory Committee for Aeronautics special report # 76".

[18] C. H. Dearborn, "The Effect of Rivet Heads on the Characteristics of a 6 by 36 Foot Clark Y Metal Airfoil," *T.N. No. 461, N.A.C.A.,* 1933.

[19] B. K. S. Joe F. Thompson, Handbook of Grid Generation, Nigel P. Weatherill, editors. CRC Press,, 1999.

[20] F. Menter, "Zonal two-equation k-w turbulence model for aerodynamic flows," *AIAA Paper 1993-2906,* 1993.

[21] P. a. S. A. s. Spalart, "A one equation turbulence model for aerodynamic flows.," *AIAA Journal,* 1992..

[22] "Fluent user manual 12.0".

[23] V. a. S. T.-H. Michelassi, "Elliptic Flow Computation by Low Reynolds Number Two-Equation Turbulence Models," *NASATM-105376,* no. CMOTT-91-11, Dec. 1991.

[24] P. J. W.-H. S. M. a. A. S. R. C. L. &. Z. L. E. G. P. Spalart, "Comments on the feasibility of LES for wings, and on a hybrid RANS/LES approach," in *1st AFOSR Int. Conf. On DNS/LES,* Aug.4-8, 1997.

[25] J. C. a. F. S. G. Patterson Jr, "An exploratory wind-tunnel investigation of the wake effect of a panel tip mounted fan-jet engine on the lift-induced vortex," *NASA TND-5729*, 1970.

[26] C. A. a. N. Markatos, "Recent advances on the numerical modelling of turbulent flows," *Computational Fluid Dynamics Unit.*

[27] D. C. Wilcox., "Turbulence Modeling for CFD," no. DCW Industries, Inc., La Canada, CA, , 1993.

[28] J. H. F. a. M. Peric, "Computational Methods for Fluid Dynamics".